Master's Thesis

$FAPbI_3$ planar heterojunction perovskite solar cells with doped zinc oxide layer

Haeyeon Kim

Department of Energy Engineering

(Energy Engineering)

Graduate School of UNIST

2017

$FAPbI_3$ planar heterojunction perovskite solar cells with doped zinc oxide layer

Haeyeon Kim

Department of Energy Engineering
(Energy Engineering)

Graduate School of UNIST

$FAPbI_3$ planar heterojunction perovskite solar cells with doped zinc oxide layer

A thesis
submitted to the Graduate School of UNIST
in partial fulfillment of the
requirements for the degree of
Master of Science

Haeyeon Kim

1. 13. 2017 Month/Day/Year of submission

Approved by

Advisor
Jin Young Kim

$FAPbI_3$ planar heterojunction perovskite solar cells with doped zinc oxide layer

Haeyeon Kim

This certifies that the thesis of Haeyeon Kim is approved.

1. 13. 2017 Month/Day/Year of submission

signature

Advisor: Jin Young Kim

signature

Hye Sung Park

signature

Sang Il Seok

Abstract

My MS research has focused on planar heterojunction perovskite solar cell as promising technology that might be renewable energy resources and the next generation flexible device. Hybrid organic-inorganic perovskite materials based on lead halides has attracted substantial attention due to their outstanding physical properties such as high absorption coefficients, excellent carrier transport with long electron-hole diffusion lengths, low exciton binding energies and easily tunable energy band gaps. These superb physical characteristics have led to high power conversion efficiencies (PCE) since the first research in solution processing perovskite solar cells (PeSCs) was reported in 2009. Perovskite solar cell has two types; n-i-p and p-i-n structures and researchers have focused on finding better method to produce uniform perovskite films with large crystal domains and complete surface coverage. And they have studied diverse approaches to improve device performance via control of the film morphology such as interface engineering, induced crystallization with non-solvents, incorporation of processing additives and so on. In the case of interfacial engineering, not only obtaining suitable interfacial condition for charge transport, but also tuning the energy band structure via doping process is still one of most widely employed techniques. In this regard, ZnO nanoparticles (NPs) have been used as an ETL in our work due to their outstanding electrical and optical properties as well as their easily controlling doping, morphology and composition compared to conventional TiO_2 ETLs. Moreover, ZnO NPs films may be coated without any thermal treatment and while ZnO possesses a higher conductivity than TiO_2, which may facilitate electron transport. Despite the advantages of ZnO compared to TiO_2, ZnO layer has a problem with methylammonium lead iodide ($MAPbI_3$, $CH_3NH_3PbI_3$). Since ZnO has a natural base characteristic, it is able to deprotonate the methylammonium cation and hence degrade the $MAPbI_3$ layer into methylamine and PbI_2 at elevated temperature.

During my research, I focused on n-i-p structures using ZnO NPs modified with various alkali metal carbonate including Li_2CO_3, Na_2CO_3, K_2CO_3 and Cs_2CO_3, which serve to tune the energy band structure of the ZnO ETL. Furthermore, I changed the $MAPbI_3$ to FAPbI3 to get higher thermal stability.

Contents

List of Figures

List of Tables

Chapter 1
Introduction

1.1 Optoelectronic device

People in the Earth using fossil fuel (coal, oil, gas, etc.), nuclear power to fill up energy need of people. These are main source of energy supply. But these sources are major cause of environmental problem, like CO_2 emission and danger of radioactive pollution. Two main reason that population and demand of energy is ongoing increased, and fuel combustion due to CO_2 emission affect global warming make people concerned. It must be commercially viable and do not create waste product like CO_2. To replace todays main source of energy with new renewable energy, researcher study next generation renewable energy like hydroelectric, wind energy, tidal power, wave power, biomass, geothermal energy, and solar energy. Among them solar energy has three main advantages that it is clean energy not to make any product, free to everyone, and sustainable for several years. Next renewable energy must be commercially viable and do not create waste product like CO_2. So solar cell is best choice. Nowadays, markets of solar cell focus inorganic silicon solar cell that are environmentally clean and high efficiency but expensive. Then from 1900s organic solar cell is alternative device of silicon cell due to several advantages, easy fabrication, low cost, low weight, and mechanically flexible. But this device doesn't have enough power conversion efficiency to be commercialized. As the result, high efficiency perovskite solar cell that almost has advantages of organic photovoltaic cell come in to the spotlight.

1.1.1 Photovoltaic device

Photovoltaic cell makes the voltage or corresponding electric current when a device gets the light that is made up packets energy, photons. They build up a voltage between two electrodes. In solar spectrum, only 45 percent of incident light energy can be used and this light is visible light range. Around 50% of light energy is Infrared range. But Ultra-violet and visible light is good to cause this phenomenon. Infrared doesn't have enough energy to make electron excited. Photovoltaic effect was discovered by French physicist Becquerel. He first found the photovoltaic effect to see a platinum electrode coated with silver bromide immersed in electrode and first found the photovoltaic effect.[1] After that, Albert Einstein invented the photoelectric effect in 1905. He observed blue ultraviolet light had enough energy that electron can escape from a metal surface completely. This effect can explain well the photovoltaic effect theoretically. Photovoltaic process has 4 steps. First is light absorption, second is charge generation, third is charge transport, and the last is charge collection. When incident light come in to a material, and this light energy is enough to make electron excite, a material absorbs the light. And absorbed incident photons hit the electron at the ground state and then make a free carrier. Free carrier

made the exciton that is bounded electron and hole. To be extracted from the material, excitons was dissociated to free charge and each free charge transports to electrode.

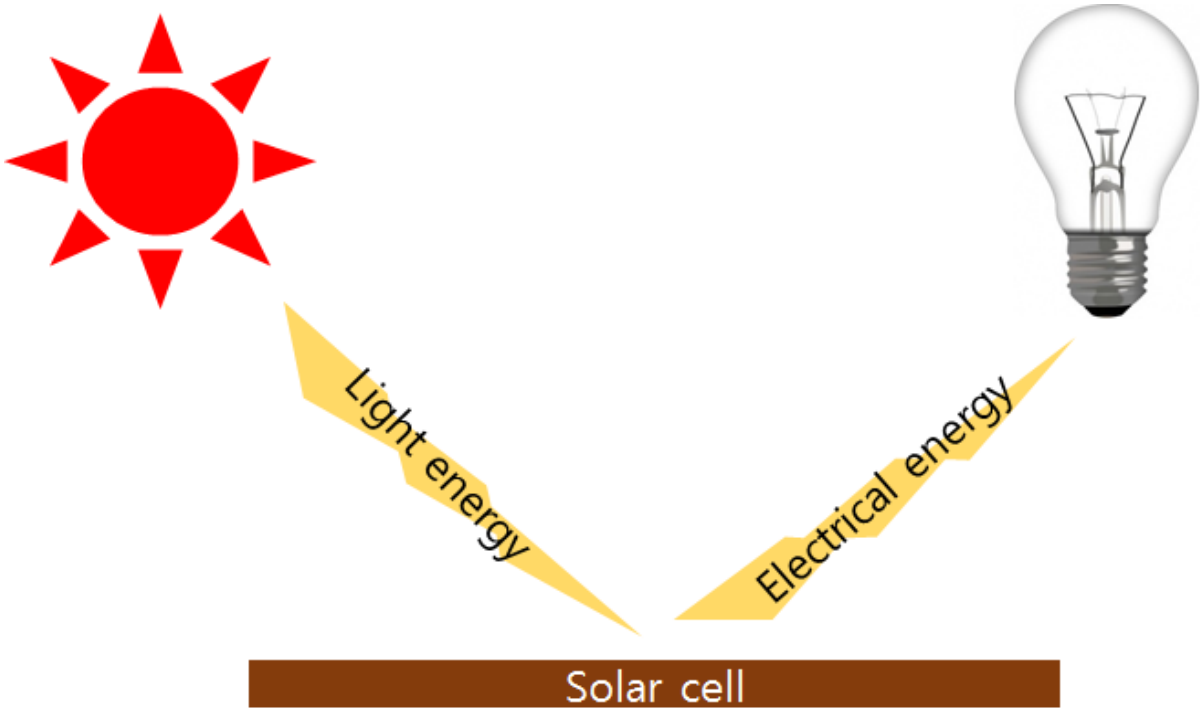

Figure 1.1 Principle of the solar cells

1.2 History of photovoltaic device.

First report of the photovoltaic device was from French physicist Becquerel in 1839 and he observed a platinum with silver coated electrode immersed in electrolyte made a photocurrent.[1] In 1876, Adams and his coworker first reported solid state Photovoltaic device that made current spontaneously without any external power supply when two heated platinum contacts met each other.[2] Pochettiro found the Anthracene, first organic material that had photoconductivity in 1906.[3] In 1950s, p-n junction in Silicon photovoltaic cell was researched, got high efficiency and used practical application.[4] In 1970s, these time occurred energy supply crisis so demands of alternative energy source were increased and attention of the photovoltaic cell was also increased. So, researcher focused to make production cost lower. Early 2000s, Alan. J. Heeger won the Nobel Prize of his research that found the organic semiconductor and established this material.[5] After Nobel Prize, people are concerned in organic photovoltaic cell. But Organic photovoltaic has two main problems; first is low diffusion length of electron and hole, and second is low dielectric constant that means it is high binding energy. Then hybrid perovskite solar cell became a viable challenger from 2009.[6]

1.2.1 History of perovskite photovoltaic cell.

First perovskite material was calcium titanium oxide mineral $CaTiO_3$ which was found from Ural Mountains of Russia by German mineralogist Gustave Rose at 1839. $CaTiO_3$ was named after Lev A. Perovski who was Russian mineralogist because he characterized this structure. Thereafter, other materials that have same crystal structure with $CaTiO_3$ were also called Perovskite structure. General perovskite material has ABX_3 chemical formula, where A and B are different size cations (A is larger than B) and X are anions.

Oxide perovskites (ABO_3) are formed by divalent cation A (Ca^{2+}, Mg^{2+}, Pb^{2+}, Ba^{2+}, Sr^{2+}) and tetravalent cation B (Fe^{4+}, Ti^{4+}, Si^{4+}) element with anion O^{2-}. They have strong character magnetic, ferroelectric, and superconductive properties.[7] Their ideal structure has B cation in 6-fold coordination, which are surrounded by an octahedron of anions (MX_3), and the A cation in 12-fold coordination. In this structure, A and B relative radii sizes are important from a tolerant factor perspective. Perovskite crystal structures were studied from 1920 by Goldschmidt who conducted tolerant factor. Tolerance factor express A-X and M-X bond lengths, $t = (R_B+R_X)/\sqrt{2}(R_A+R_X)$ (R_A, R_B, R_X are the ionic radii of A, B, and X, respectively).[8] Structures are stable when t approaches 1. Using this value, researchers have found the proper tuning of composition. First oxide perovskite $BaTiO_3$ generated photocurrent at 1956, and then $LiNbO_3$ generated similar phenomenon.[9] From these pioneering studies, researcher began to study possibility of the photovoltaic application in these oxide perovskites. However oxide perovskites have higher energy band gap, so it is not adaptable to photovoltaic cell.[10]

Halide perovskites (ABX_3) are firstly formed from the monovalent alkali metal cations A (Cs^+, Li^+, Na^+, K^+, Rb^+) and the divalent cations B (Be^{2+}, Ni^{2+}, Mg^{2+}, Co^{2+}, Ca^{2+}, Fe^{2+}, Sr^{2+}, Pb^{2+}, Ba^{2+}, Sn^{2+}, Zn^{2+}, Ge^{2+}) with halogen anions X (F^-, Cl^-, Br^-, I^-). And this has lower energy band gap than oxide perovskites. Until 1980, there was no report that halide perovskites materials were used to solar absorbers. Salau reported a new halogen perovskite, potassium lead iodide ($KPbI_3$) that has a direct energy band gap between 1.4 and 2.2 eV). The writer suggested these new materials proper to photovoltaic cell because that energy gap well matches the solar spectrum. This new solar cell material was anticipated that theoretical efficiency is about 36% and operating temperature is 220^{o}C. But he didn't realize any real solar cell.[11]

Independent of alkali metal halide perovskite, organometal halide perovskites (ABX_3) are studied for the past 20 years. ABX_3 consist of organic cations A (aliphatic or aromatic ammonium like methylammonium, MA^+ or formamidinium, FA^+) and the divalent cations B (Cu^{2+}, Ni^{2+}, Cd^{2+}, Co^{2+}, Fe^{2+}, Pb^{2+}, Mn^{2+}, Sn^{2+}, Pd^{2+}, Eu^{2+}) with halogen anions X. Among these B cations, researcher focus the fourth main group 4A (Ge^{2+}, Sn^{2+}, Pb^{2+}) due to their two main advantages that it is possible to fabricate devices at low temperature and it has good optoelectronic properties. For decades, perovskite material drew initial interest for light-emitting diode (LED) and thin film transistor (TFT) application due to their photo or ionic conductivity and semiconducting properties.[12] At the same time, lead based halide perovskites and tin based halide perovskites received less attention because it has much less chare

carrier mobility and metallic behavior.[13]

In the 2009, Miyasaka realized first organometal halide perovskite photovoltaic cells. They induced methylammonium lead halogen ($CH_3NH_3PbX_3$, X: Cl, Br) as visible-light sensitizes on mesoporous TiO_2 in a dye sensitized solar cell (DSSC) with liquid electrolyte. This device's power conversion efficiency (PCE) was 3.8%.[6] Subsequently, Park and coworkers fabricated liquid electrolyte based DSSC using $CH_3NH_3PbI_3$ and gained the 6.5 % of PCE in 2011.[14] In 2012, M. Gratzel used solid electrolyte spiro-OMeTAD (2,2'7,7'-tetrakis(N,N-di-p-methoxyphenylamine)-9,9'-spirobiflurene) as hole transport material (HTM) and they achieved 9.7% efficiency and stability of this cell was increased due to solid HTM.[15] After that, H. Snaith discovered meso-superstructured solar cells that replace n-type TiO_2 electron transport material (ETM) with an inert Al_2O_3 scaffold, which get to a 9.7% efficiency.[16] After that time, researcher focused on perovskite solar cell field.

Chapter 2

Background of Perovskite solar cells

This chapter will be covered the general information of perovskite solar cells on structures, device architecture, and important parameters.

2.1Perovskite composition

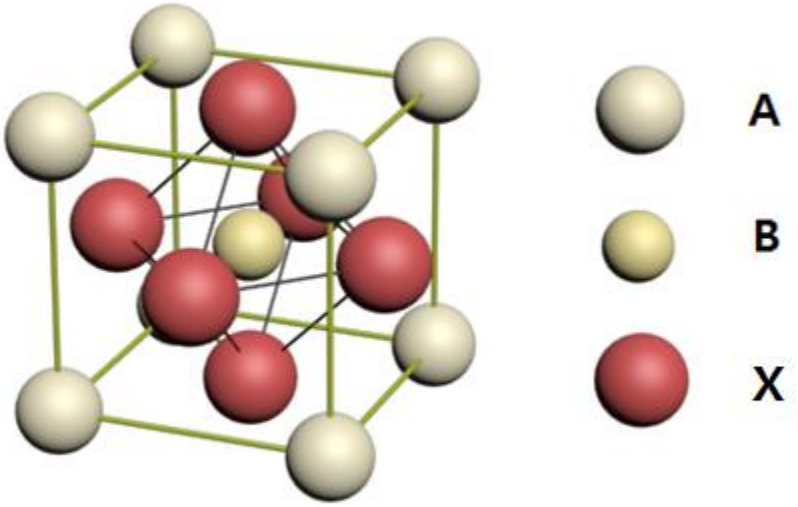

Figure 2.1 Crystal structure of the perovskite materials

2.1.1 Influence of A cation

A cation doesn't directly contribute the band structure and electronic property. But size of A cation change the degree of the distortion, electronic property get the effective.[17] And optical properties are affected due to variation of its size. Size of cation can affect the whole lattice to contract or expand and change the B-X bond length that play an important role in determining the band gap.[18,19] A lattice site is filled by small monovalent cation A, such as methylammonium (MA), cesium (Cs), ethylammonium (EA), formamidinium (FA). As R_A increasing, tolerant factor (t) approaches 1, and make higher packing symmetry and then smaller energy band gap. Since A cation must fit in the corner-sharing metal halide octahedral, it has relatively smaller size range. When t=1, R_A must not be larger than 0.26 nm due to maintain cubic symmetry. Candidates for A cation sizes are $R_{Cs}<R_{MA}<R_{FA}<R_{EA}$.[20]

MA is widely used cation for hybrid perovskite solar cell with R_{MA} =0.18 nm.[21] At room temperature,

$MAPbI_3$ retains tetragonal symmetry due to small size, and then it gets 1.51-1.55 eV of energy gap. By decreasing R_A, perovskite yields the smaller band gap corresponding to get light harvesting.[22,20,23] But Replacement MA with excessively large cation EA(R_{EA}=2.3 Å) makes 3D symmetry changed to 2 D orthorhombic crystal and yields larger energy band gap 2.2eV.[24] FA yield a higher symmetry than EA. FA-I ion interaction is natively disordered so $FAPbI_3$ has trigonal structures. And its band gap is closer to optimal band gap 1.4 eV of solar cell, 1.34~1.48 eV.[22,25,26] Cs is smaller size cation (R_{Cs}=1.67 Å), and make octahedral tilting resulting in t reduced (lower symmetry). $CsPbI_3$ has higher energy gap 1.73 eV.[20]

Ion	EA	FA	MA	Cs
Ionic radius (Å)	2.3	1.9-2.2	1.8	1.67

Table 2.1 Ionic radii of A cation.

2.1.2 Influence of B cation

In B sites, fourth main group 4A cation with divalent oxidation state (Ge^{2+}, Sn^{2+}, Pb^{2+}) are sited. In Germanium (Ge) case, $AGeX_3$ has been studied rarely due to unstable 2+ oxidation state.[27,28,29] In the perovskite ABX_3 structure, X-B-X bond angle affect the energy gap. Each B-I-B angles in MI_6 structure are 166.27° of Ge, 159.61° of Sn and 155.19° of Pb.[30] At the same time, reduction of covalent character of B-I that means increasing difference between electron-negativity of B and I yields growth of energy gap. So, energy gap of ABI_3 is $AGeI_3$<$ASnI_3$<$APbI_3$. $MASnX_3$ energy gap is range between from 1.2 to 1.4 eV and more optimum than $MAPbX_3$ that has energy gap between 1.6-1.8 eV.[28,29,31] But Sn^{2+} is well oxidized to Sn^{4+} under air condition that means Sn based perovskite is very sensitive in air.[32] So Until now, although tin based perovskite solar cell has been expected to get higher photocurrent density, lead based perovskite solar cell is focused by researchers.

2.1.3 Influence of X anion

As down in VIIA group (Cl→Br→I), atomic size of anion is decreased resulting in growth of lattice constant. Accordingly, electron-negativity is decreased. Also, decline of electron-negativity yields the increasing covalent character. And incline covalent character make energy gap red shift.[32] Iodide (I) has similar covalent character with Pb because iodide position in the periodic table is closer to Pb. So $APbI_3$ structure is most stable and widely used. Chloride (Cl) improves the diffusion length and carrier life time. Tuning the Cl to $APbI_3$ retain the same energy gap with pure iodide structure. Ionic radii and covalent character of Cl are largely different with those of I. As the result, tuning Cl ions with I ions is difficult. Mixed $MAPbI_{3-X}Cl_X$ has highly oriented crystalline structure due to Cl doping.[33,34,35] Bromide (Br) are used to tune the energy band gap of the $APbI_3$. Due to larger ionic radii of Br than that of I, Br

make a compressive stress on Pb-I bonds, and its stress make the distortion of the structure.[36,33] Simultaneously it leads increasing the band gap. In case of Fluoride (F), it was expected to be good optoelectronic device, however, its strong hydrogen bonding (N-H-F) cause a disagreeable tolerance factor and high degree of strain.[37,38]

Ion	I	Br	Cl	F
Ionic radius (Å)	2.2	1.96	1.81	1.33

Table 2.2 Ionic radii of X cation.

2.2 Perovskite solar cell

2.2.1 Device of architecture

Perovskite solar cell was originally initiated from dye sensitized solar cell (DSSC). Researcher changed from the conventional dye to perovskite material.[6] After that they use mesoporous TiO_2 scaffolds. On transparent conductive oxide (TCO), compact TiO_2 is covered and then mesoporous $TiO_2$is stacked on it. Perovskite material is infiltrated on mesoporous TiO_2 scaffold about 350 nm. Due to their thickness, perovskite absorbs a great part of incident photons.[25,39] TiO_2 block has been studied so researcher changed the block to nanowire, nanorod, nanocones, nanofibers, nanotubes, nanohelics.[40,41,42,43,44] Around the same time, insulating scaffold of Al_2O_3 was induced the cell to achieve adaptable PCE. But after further study, perovskite already has better transport of both electron and hole resulting in not necessary for mesoporous scaffold. To make simple device, researcher designed the planar heterojunction perovskite solar cell that was sandwiched between hole and electron transport layer (HTL, ETL). Planar configuration has two categories, n-i-p and p-i-n structure. n-i-p structures are glass/TCO/ETL/perovskite/HTL/metal, the other way, p-i-n structures are glass/TCO/HTL/perovskite/ETL/metal.[45-46] In that structure, researchers focus on two issues due to simple structure. First is finding better HTL and ETL and interface engineering. Second is a deposition technique to make proper film. Other configuration is perovskite/BHJ (bulk heterojunction).[47]

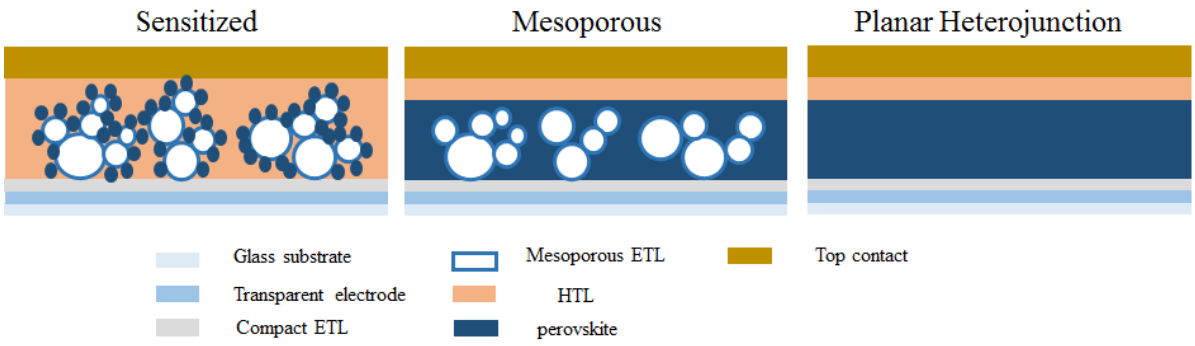

Figure 2.2 Three major device architectures of perovskite solar cells.

2.2.2 First issue

Hole transport material

HTM has been studied since appearance of perovskite solar cell because perovskite solar cell was comprised from DSSC and that structure use TiO_2. HTM has various types, organic small molecules, oligomers, polymers, inorganic crystal. In organic small molecules case, 2,2',7,7'-Tetrakis[N,N-di(4-methoxyphenyl)amino]9,9'-spirobifluorene (spiro-OMeTAD) was used as HTM from 2012.[15] Pristine spiro-OMeTAD has low electric conductivity, then it was chemical doped to increase carrier concentration and conductivity.[48,49] And researchers have developed other new small molecule HTM. Among them, there was acceptor-donor-acceptor (A-D-A) type small molecules like OPV.[50,51] Among them, there was M1 that has benzo[1,2b:4,5b']-dithiophene (BDT) donor and a phenoxazine (POZ) acceptor.[52] Conjugated polymer also has been studied. Among them, PEODT:PSS has various advantages; excellent transparency, adaptable work function, high conductivity, and good chemical stability. But PEDOT:PSS is used at inverted configuration due to their water based characteristic.[53] But it has relatively low difference of work function between perovskite and itself. Another conjugated polymer is poly(3-hexylthiophene-2,5-diyl) (P3HT) that has many advantages; excellent electrical property, dense structure, and easy processing.[54] Poly-triarylamine (PTAA) is pillared structure and that has 12% PCE at 2013. It has higher open circuit voltage (V_{oc}) and fill factor (FF) due to adaptable energy level and conductivity.[53] And then other polymer has been used as HTM. Inorganic HTM has high stability and low cost than others. CuI has high short circuit current density (J_{sc}), FF and stable photocurrent, but it has lower V_{oc} due to severe recombination.[55] NiO was first reported metal oxide as HTL. It was used as p-i-n structure like PEDOT:PSS, and then it has higher quality than PEDOT:PSS as regards it has better wetting and energy alignments.[56] CuSCN that has high hole mobility, better chemical stability and solution process got the 12.4% efficiency at 2014.[57,58]

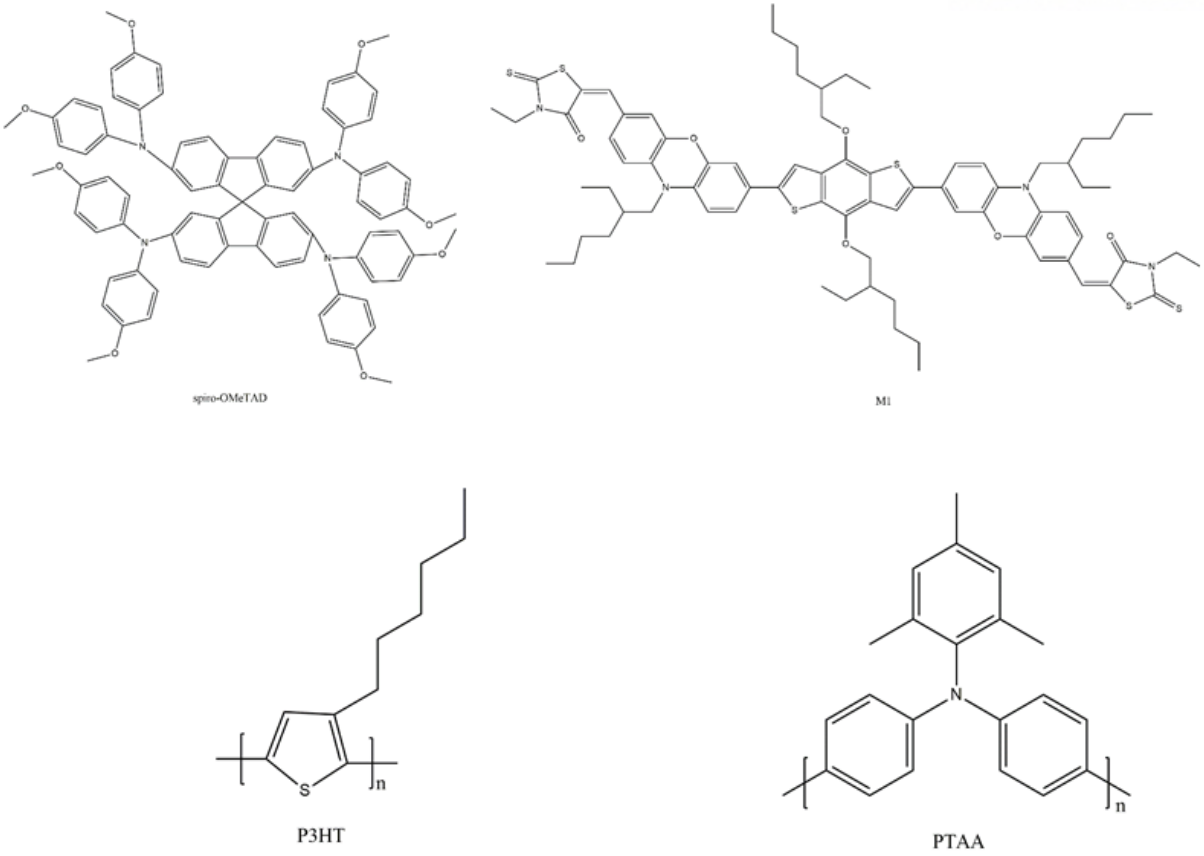

Figure 2.3 Major organic hole transport materials.

Electron transport material

TiO_2 has been studied from DSSC and it extracts electron well, and retards recombination of holes at electrodes. But compact TiO_2 has to be annealed up to 450°C.[16] To avoid high annealing temperature, researchers found the sol-gel process of making TiO_2.[59] And ZnO has new alternative ETM that used as electron selective contact.[60] $PC_{60}BM$ has been well used with PEDOT:PSS, and it makes PL quenching. $P_{71}BM$ has higher J_{sc} and FF than $PC_{60}BM$ due to better response in visible region.[61] To get higher PCE, researchers used double fullerene layer, which was PCBM/C_{60} layer; C_{60} layer was thermal evaporated after PCBM was spun coating. It eliminated the leakage current and compensate the passivation of trap.[62] And ETL has been studying nowadays.

Interfacial modification

To control behavior of carriers and retard to age the interface due to improvement of device stability, researchers have modified the interfacial. Abete et al. used iodopentafluorobenzene (IPFB) inserted between perovskite and HTM to increase hole extraction. And there are several try to passivate the TiO_2 surface. C_{60}-SAM modified the TiO_2 to reduce non-radioactive recombination. Graphene quantum dot

was inserted between perovskite and TiO_2 to reduce electron extraction time and change the electrode. In case of PEIE, it was coated on TCE to reduce the TEC work function then schottky barrier was impossible to occur between electrode and perovskite. Zwitterionic small molecule and LiF changed the electron transport of cathode. LiF was inserted beneath Ag electrode to increase V_{oc}. $Cs_2CO_3$was also changed the energy level alignment of ITO. Other interfacial layer like poly[(9,9-bis(3'-(N,N-dimethylamino)propyl)2,7-fluorene)-alt-2,7-(9,9-ioctylfluorene)] (PFN) and batocuprioine (BCP) are good at collecting electron, result in change of cathode. On the stability point, Sb_2S_3 was inserted between $TiO_2$and perovskite layer to increase the device stability about the light. On the illumination, it made less degradation to format PbI_2. Al_2O_3 also retarded the perovskite decomposition.

2.2.3 Second issue; deposition technique

Deposition of perovskite is repetition of nucleation and growth. Researcher focused to get high quality film resulting from changing morphology, crystallinity, and optoelectronic property. The key point of the change 4 factors; first is deposition method, second is surrounding environment, and then third is precursor composition. Final is solvents and additive used. High quality film has been studying about precursor stoichiometry, thermal treatment, additives, atmosphere, and solvent engineering.[47]

Techniques of film formation

Largely, there was three deposition processes according to precursor: vacuum, solution and hybrid. First is vacuum deposition. In that deposition, there are two processes. First is co-evaporating of organic and inorganic compound.[63] The other is a sequential vapor deposition that $PbCl_2$ was first deposited and then followed MAI.[64] Second is solution processing. This process has been usually used due to easy process and low cost. In that process, there are two process, single step and two step sequential deposition method.[25, 65] On the mesoporous scaffold, both made adaptable layer. But under the planar configuration, one step method was not adaptable due to surface energy and nucleation.[16] Third is hybrid vapor-solution process that is firstly suggested by Chen.[66] PbI2 layer was first deposited by spin coating and then MAI coating by vapor. As result, lμm of grain was obtained and surface roughness was reduced.

(a) Vacuum process

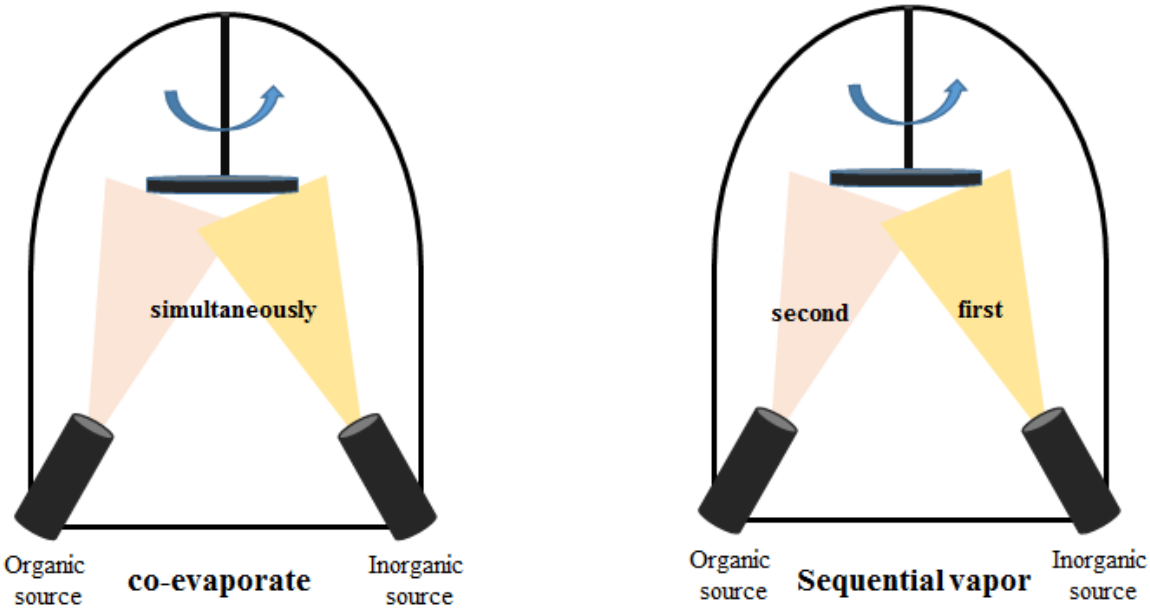

(b) Solution process

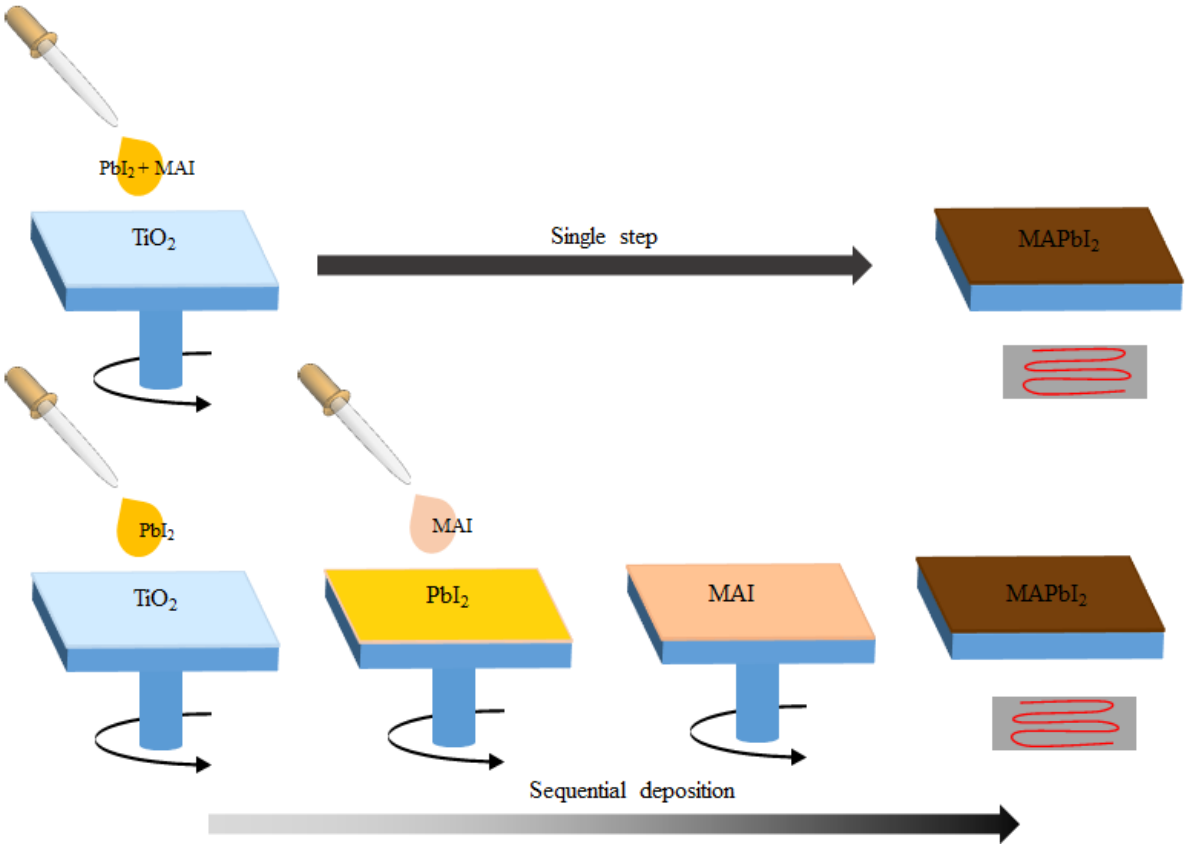

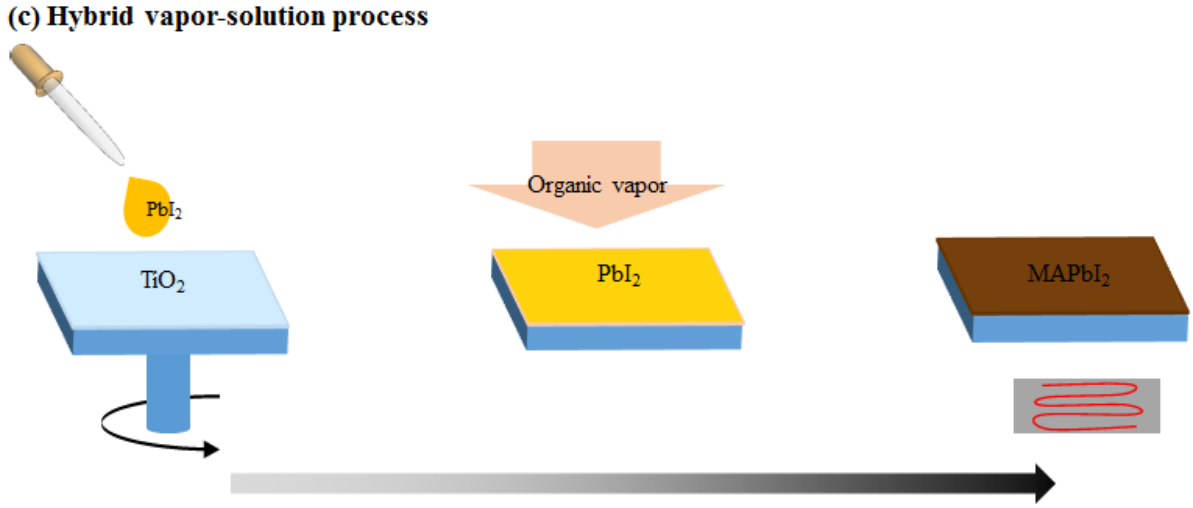

Figure 2.4 Different deposition methods of Perovskite films.

Precursor stoichiometry

The ratio of organic compound and inorganic compound affect the quality of perovskite layer. Usually 3:1 and 1:1 ratio of perovskite precursor has been used. Originally 1:1 ratio is suitable ratio through stoichiometry. But in the single step deposition, this film didn't have full coverage. As the result, researcher found the new ratio to solve the problem of the coverage, that ratio is 3:1. 3:1 ratio of $MAPbI_{3-x}Cl_x$ has larger grain size than $MAPbI_3$ and film quality was improved.[16] And then $MAPbI_{3-x}Cl_x$has higher carrier lifetimes, 100ns than $MAPbI_3$ of ions.[35] In that case, perfect $MAPbI_3$layer could be obtained through MAI:$PbCl_2$=3:1 ratio. In the planar $MAPbI_3$ structures, non-stoichiometric precursor solution is used to get high quality film.[67] According to PbI_2 to MAI ratio, at lower 0.6 of $PbI_2$to 0.1 of MAI ratio (<0.6:0.1) couldn't fully cover resulting in no photoluminescence peaks and absorption edges due to excess $MAPbI_3$. At higher 0.8 PbI_2 to 1 of MAI ratios (>0.8:1) format the microfibers, so roughness was increased. Recently other researcher team showed excess organic compound make colloidal size reduced and substitution of small amount of chlorine make crystalline nucleation accelerated.[68] To get high quality film, stoichiometry has been deeply considered by many researcher teams.

Thermal treatment

Thermal treatment is necessary to initiate the reaction for making perovskite structures. Eperon compared the morphology of perovskite layer through annealing temperature with $MAPbI_{3-x}Cl_x$ based planar perovskite structure.[20] They controlled the temperature from 90 °C to 170 °C. With high annealing temperature, surface couldn't be fully covered. Dualeh annealed the substrate at 80 °C for 30 min and 100 °C for 45 min respectively. Longer annealing time at low temperature couldn't make any advantages of the film quality. Saliba reported the annealing at higher temperatures for shorter times. As that result,

recombination losses are reduced at grain boundaries.[69] Thermal annealing also affects two steps sequential.

Additives

Adding small amounts of additives in precursor solution affect the perovskite layer characteristic; crystallinity and film coverage. 1% of 1,8-diiodocatane (DIO) was added into precursor solution surface coverage and crystallinity were improved. They expected that I^- ligand of DIO affect the perovskite structures and made solubility of $PbCl_2$ high.[70] Zuo added the NH4Cl in precursor and get the high performance resulting from high crystallinity and film morphology.[71] Chen added the 3% of small molecule BmPyPhB in precursor solution to help the formation of perovskite.[72]

Atmospheric effects

Perovskite degraded when they face to moisture, researchers usually make the perovskite layer on the nitrogen glove box. But recently, it was reported that perovskite annealed on moderate moisture condition has better film quality.[73] V_{oc} are influenced by the amount of moisture. You reported that moisture make the grain larger resulting in from motion of organic species. So perovskite layer with annealed at ambient air has larger grain sizes.[74] Xiao try the solvent vapor annealing to optimize the layer morphology. He annealed the perovskite layer at 100 ^oC for 1 hours at DMF vapor condition. It helps interaction between PbI_2 and MAI.[75]

Solvent engineering

The choice of solvent is important to make the perovskite layer. Usually researchers has been used N,N-dimethylformamide (DMF), Y-butyrolactone (GBL) and dimethyl sulfoxide. Solvents have different parameter each other like boiling point, viscosity, and solubility. Solvent type affect the perovskite quality, so many researchers focused on finding adaptable solvent. Researcher used the DMF (b.p. 154 ^oC) replacement of GBL (b.p. 204 ^oC) result from high quality film. But $MAPbI_3$ growth rate is faster than formation rate of pin holes.[59] Then solvent-wash has been used to make dense perovskite films. Organic solvent was dropped on the wet perovskite film to lead to fast crystallization. It controlled the factor of kinetic of nucleation.[76,77] Other researcher used a small amount of GBL in DMF solution to reduce the growth rate. GBL and DMSO mixture solvent was used. They used toluene to freeze the MAI-PbI_2-DMSO and remove the excess DMSO. Nowadays, researcher has been focused on optimized the film morphology.[76]

Chapter 3

$FAPbI_3$ planar heterojunction perovskite solar cells with alkali carbonate doped zinc oxide layer

3.1. Introduction

Considerable effort to develop renewable energy sources has been expended over the last several decades, leading to the demonstration of several new classes of highly efficient photovoltaic cells. Inorganic, organic and hybrid light absorbers such as organic bulk heterojunctions, colloidal quantum-dots and dye-sensitized metal oxide devices have been demonstrated as next generation photovoltaic materials.[14] However, the emerging class of hybrid organic-inorganic perovskite materials based on lead halides has have attracted substantial attention due to their outstanding physical properties such as high absorption coefficients, excellent carrier transport with long electron-hole diffusion lengths, low exciton binding energies and easily tunable energy band gaps. These superb physical characteristic have led to high power conversion efficiencies (PCE) since the first research in the area of solution processing perovskite solar cells (PeSCs) was reported in 2009.[6]

To achieve highly efficient PeSCs, the perovskite layer must be deposited with a uniform, highly-crystalline and dense morphology, which completely covers the underlying surface. Diverse methods such as vapor-assisted deposition, solvent engineering and intermolecular exchange have been introduced to produce uniform perovskite films with large crystal domains and complete surface coverage.[66, 76, 78] Diverse approaches to improve device performance via control of the film morphology have been introduced, such as via interface engineering, induced crystallization with non-solvents, incorporation of processing additives and so on.[79-80] In the case of interfacial engineering, not only obtaining suitable interfacial condition for charge transport, but also tuning the energy band structure via doping process is still one of most widely employed techniques.[81-85] Recently, Nho et al. reported that addition of metal carbonate led to improvement of the electron extracting properties of zinc oxide (ZnO) layer via modification its energy levels.[86] This result suggests that metal carbonates may be applied to improve device performance if the energy level of doped electron transport layer (ETL) is matched with the conduction band of the perovskite active layer.

In this regard, ZnO nanoparticles (NPs) have been used as an ETL in our work due to their outstanding electrical and optical properties as well as their easily controlling doping, morphology and composition compared to conventional TiO_2 ETLs.[87-88] Moreover, ZnO NPs films may be coated without any thermal treatment and while ZnO possesses a higher conductivity than TiO_2, which may facilitate electron transport.[89-90] However, the highest device efficiency using ZnO ETLs to date has only reached 17.1%, compared to TiO_2 based ETLs which have achieved over 20% PCE, suggesting

that there is considerable room to improve the performance of ZnO based devices.[78, 91]

Despite the advantages of ZnO compared to TiO_2, ZnO layer has a problem with methylammonium lead iodide ($MAPbI_3$, $CH_3NH_3PbI_3$). In previous literature about ZnO based perovskite solar cell, Yang et al. reported that the ZnO layer reacted with $MAPbI_3$ in an acid-base reaction upon annealing the devices.[92] Since ZnO has a natural base characteristic, it is able to deprotonate the methylammonium cation and hence degrades the $MAPbI_3$ layer into methylamine and PbI_2 at elevated temperature. For these reason, Song et al. reported $FAPbI_3$ which is an alternative materials to $MAPbI_3$ has more thermal stability due to difficulty of the deprotonation process.[93] Moreover, $FAPbI_3$ has several key advantages; lower band gap, improved stability and weaker hysteresis due to well-balanced electron and hole transport compared to $MAPbI_3$.[94]

Herein, we demonstrate n-i-p type planar heterojunction perovskite solar cells employing spin-coated ZnO nanoparticles modified with various alkali metal carbonate including Li_2CO_3, Na_2CO_3, K_2CO_3 and Cs_2CO_3, which serve to tune the energy band structure of the ZnO ETL. Since these doped metal carbonate series on ZnO ETL lead the deeper conduction band of ZnO ETL, the electron easily transport from perovskite active layer to cathode electrode. PCEs were improved from 11% to 14%, via incorporation of alkali carbonates in the ETL.

3.2 Comparison between $MAPbI_3$ and $FAPbI_3$.

To get further information about the thermal stability at the interface between perovskite layer and ZnO, we deposited perovskite layer on ZnO and heated substrates. In this study, MAI and FAI solutions were dripped onto PbI_2 substrates that already deposited by spin coating and then spin coated to form perovskite layer in a nitrogen atmosphere. Films were converted to perovskite structures after annealing the substrates.

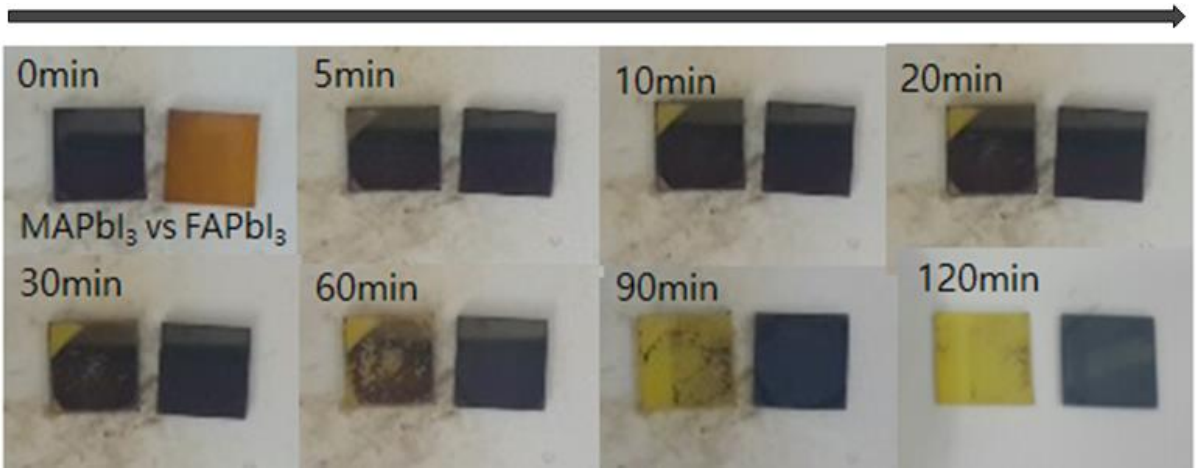

Figure 3.1 Thermal stability of $MAPbI_3$ and $FAPbI_3$ deposited on ZnO layer, when each substrate is annealed in N_2 at 100°C for the times indicated.

To compare the thermal stability of $MAPbI_3$ and $FAPbI_3$ perovskite, we simultaneously gave heat each cell on a hot plate at a temperature of 100 °C. **Figure 3.1** compares the thermal stability of $MAPbI_3$ and $FAPbI_3$ on ZnO. After 10 min. of heating, we observed that $MAPbI_3$ films had decomposed to MAI and PbI_2 at the edges, as indicated by yellow color. The decomposition region gradually increased over 90 min. until the entire $MAPbI_3$ film changed from dark brown to yellow. In contrast, after 120 min., the $FAPbI_3$ film did not exhibit any visible decomposition and the color remained dark unchanged, indicating that $FAPbI_3$ has better thermal stability with ZnO than $MAPbI_3$. Except thermal stability, this report marks the study to utilize a formamidinium-based active layer in conjunction with a ZnO ETL. Formation of uniform $FAPbI_3$ film was difficult due to large cation size of FA^+. We optimized each perovskite layers on the ZnO.

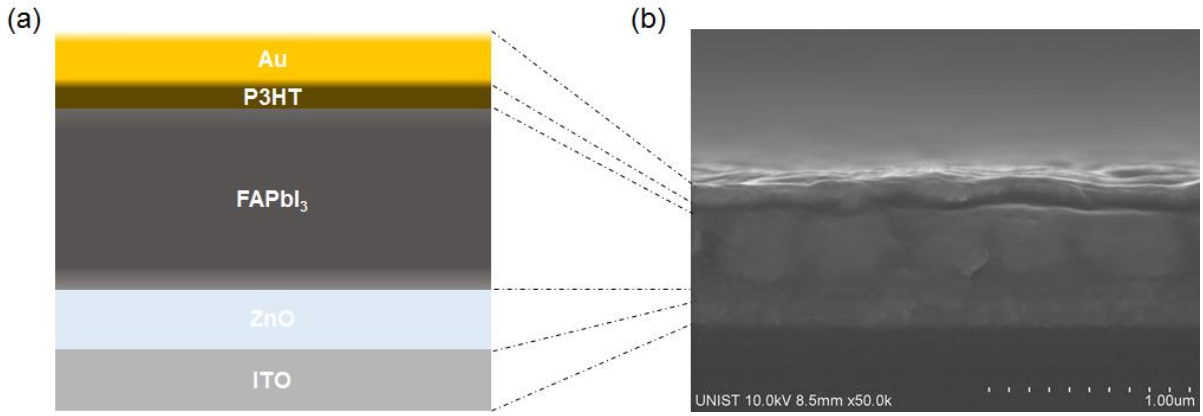

Figure 3.2 (a) Schematic diagram and (b) SEM cross section images of the conventional planar perovskite solar cells using doped ZnO.

Figure 3.2a presents a schematic diagram of the device architecture used in this study comprising sequentially deposited ZnO/perovskite/poly(3-hexylthiophene-2,5-diyl)(P3HT)/Au on indium tin oxide (ITO) substrates compared perovskite between $MAPbI_3$ and $FAPbI_3$. In **figure 3.2b**, a cross-sectional scanning electron microscope measurements (SEM) image shows the complete device stack revealing that the perovskite materials fully coat the ZnO layer without any defects.

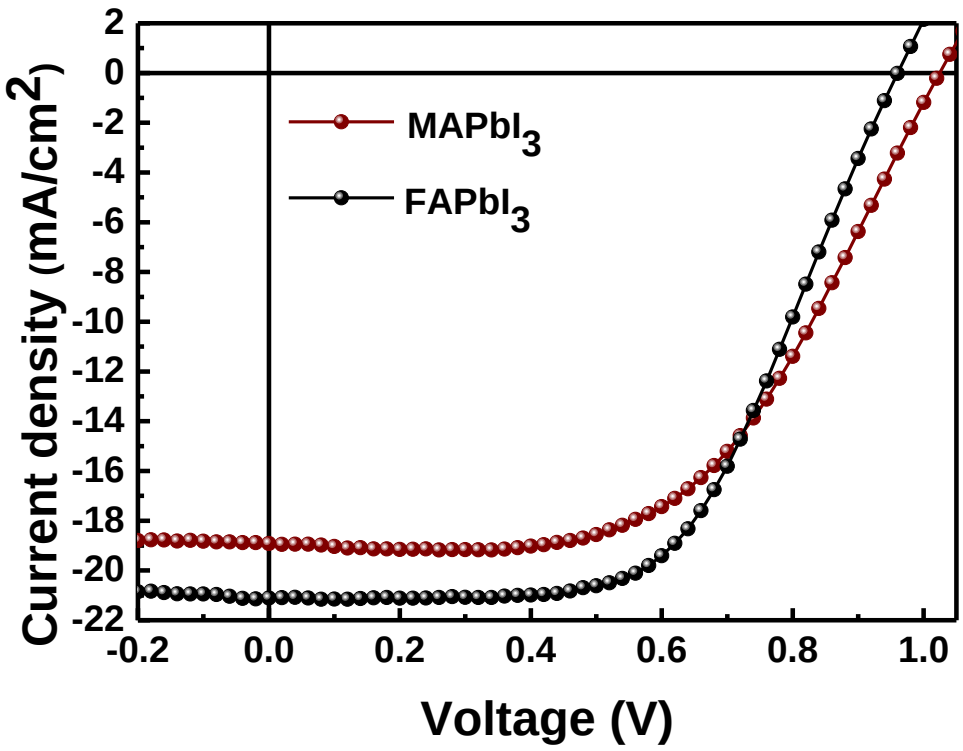

Figure 3.3 Current density – voltage characteristics of $MAPbI_3$ and $FAPbI_3$ planar solar cells under 100mW cm^{-2} AM1.5 illumination.

	J_{SC} (mA/cm^2)	V_{OC} (V)	*FF*	PCE (%)	Cal. J_{sc} (mA/cm^2)
$MAPbI_3$	18.9	1.02	0.55	10.7	17.5
$FAPbI_3$	21.1	0.96	0.58	11.7	19.7

Table 3.1 Solar cell characteristic of $MAPbI_3$ and $FAPbI_3$ devices.

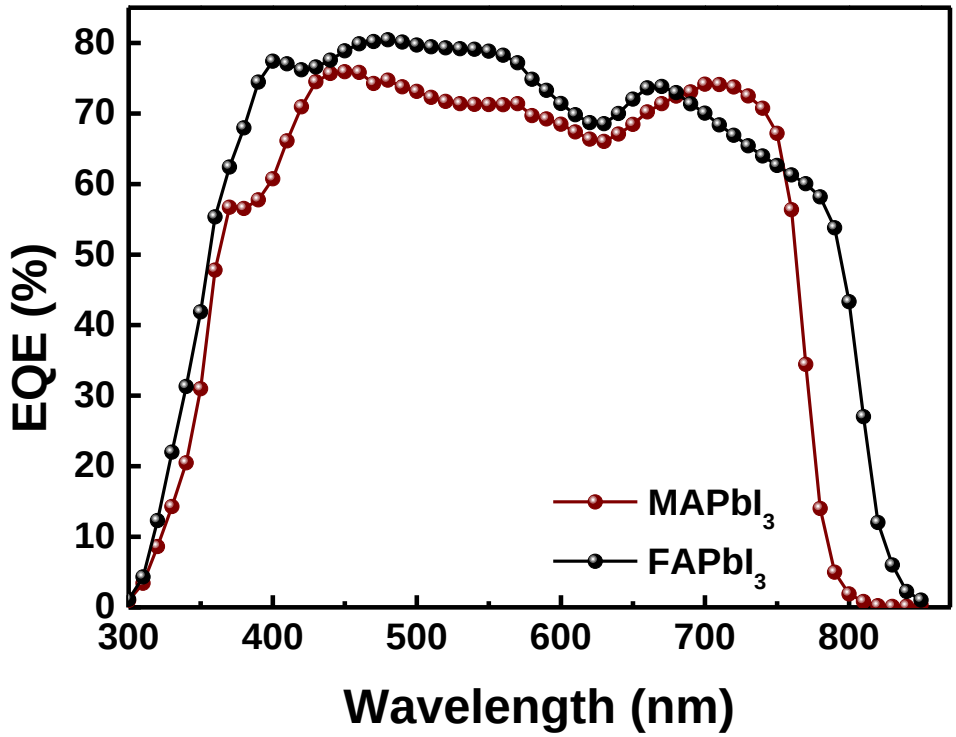

Figure 3.4 External Quantum Efficiency spectra of each of $MAPbI_3$ and $FAPbI_3$ device.

Figure 3.3 shows the current density-voltage curve of $MAPbI_3$ and $FAPbI_3$ solar cell has had lower short circuit current density (J_{sc}) of 18.9 mA cm^{-2}, higher open circuit voltage (V_{oc}) of 1.02 V, and fill factor (FF) of 0.55. This device yielded power conversion efficiency (PCE) of 10.7 %. On the other hand, $FAPbI_3$ solar cell had higher J_{sc} of 21,2 mA cm^{-2}, shorter V_{oc} of 0.96 V, FF of 0.58 and PCE of 11.7 % (**Table 3.1**). FAPbI3 has a closer bandgap to the Shockley-Queisser maxim, 1.40 eV, so J_{sc} was increased. **Figure 3.4** shows External Quantum Efficiency (EQE) spectra that displayed the absorption edge about 870 nm of $FAPbI_3$ is higher than $MAPbI_3$ about 800 nm. Addition to the optimization of perovskite layer, we found modifying ZnO layer with metal carbonates led to excellent performance.

3.3 ZnO doped with metal carbonate

We demonstrated n-i-p type planar heterojunction perovskite solar cells employing spin-coated ZnO nanoparticles modified with various alkali metal carbonates including Li_2CO_3, Na_2CO_3, K_2CO_3, and Cs_2CO_3, which serve to tune the energy band structure of the ZnO ETL. Since these doped metal carbonate series on ZnO ETL lead the deeper conduction band of the ZnO ETL, the electron transport from perovskite active layer to cathode electrode due to low energy barrier. PCEs were improved from 11% to 14%, via incorporation of alkali carbonates in the ETL.

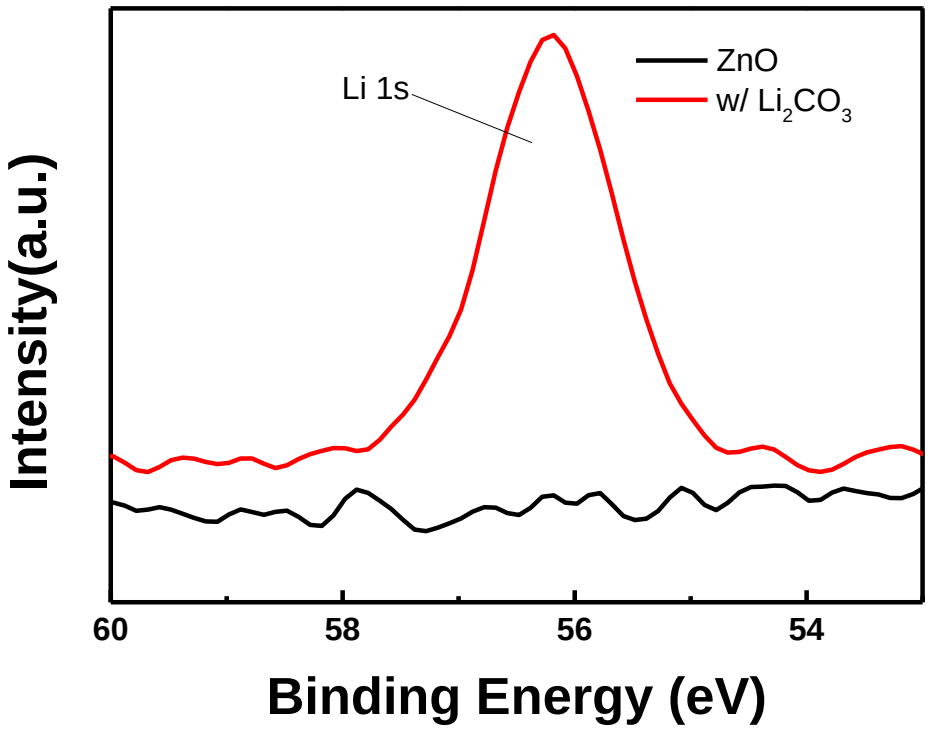

Figure 3.5a X-ray photoelectron spectra (XPS) data of the Li peak compared between pristine ZnO layer and ZnO doped with Li_2CO_3 layer.

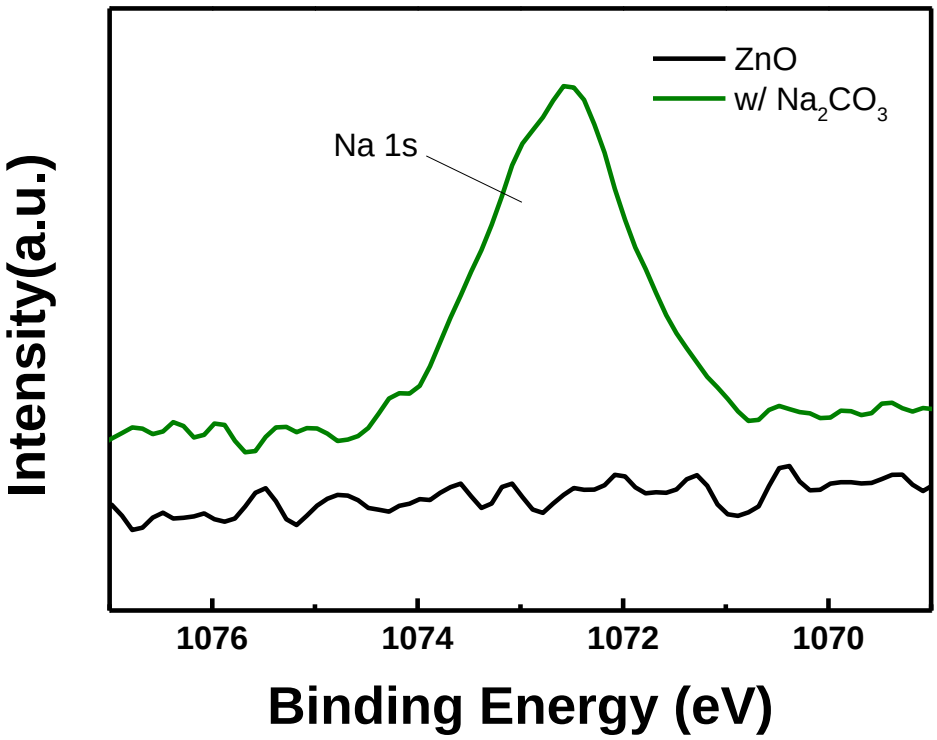

Figure 3.5b X-ray photoelectron spectra (XPS) data of the Na peak compared between pristine ZnO layer and ZnO doped with Na_2CO_3 layer.

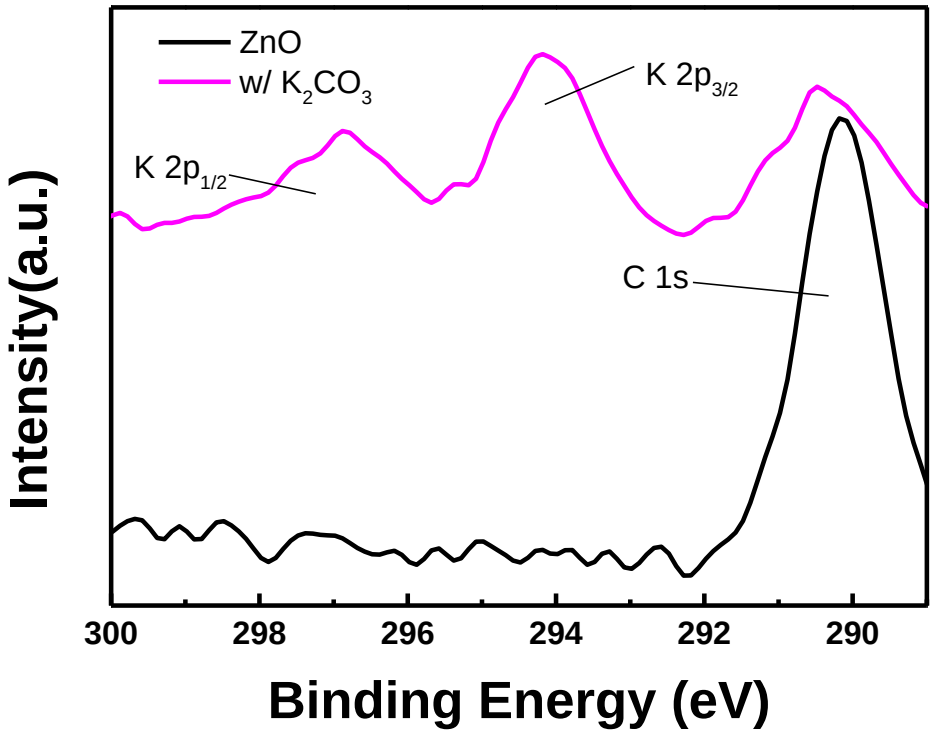

Figure 3.5c X-ray photoelectron spectra (XPS) data of the K peak compared between pristine ZnO layer and ZnO doped with K_2CO_3 layer.

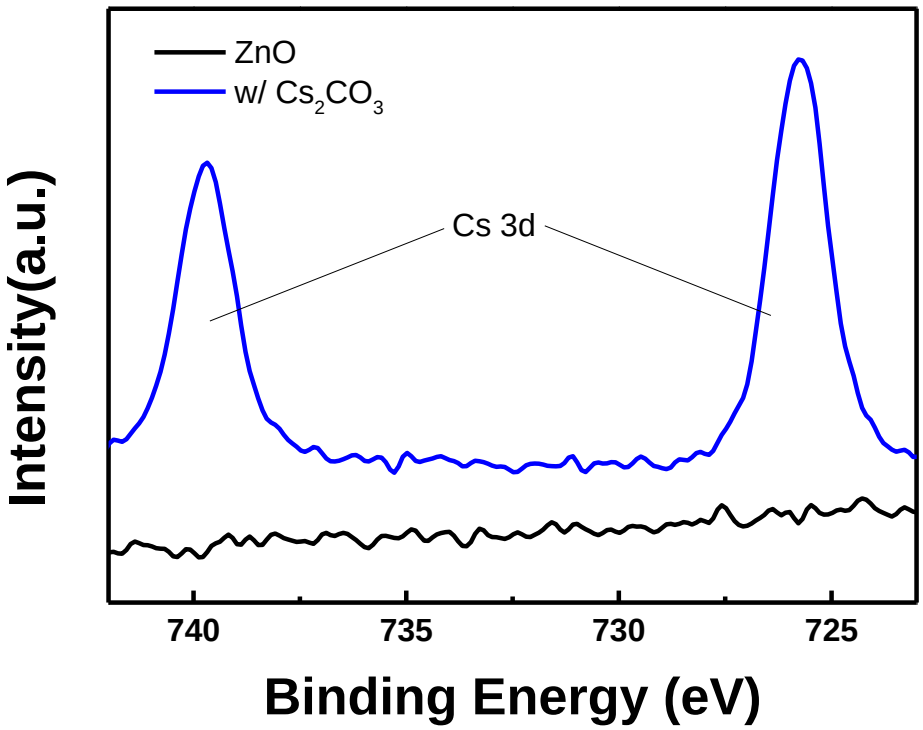

Figure 3.5d X-ray photoelectron spectra (XPS) data of the Cs peak compared between pristine ZnO layer and ZnO doped with Cs_2CO_3 layer.

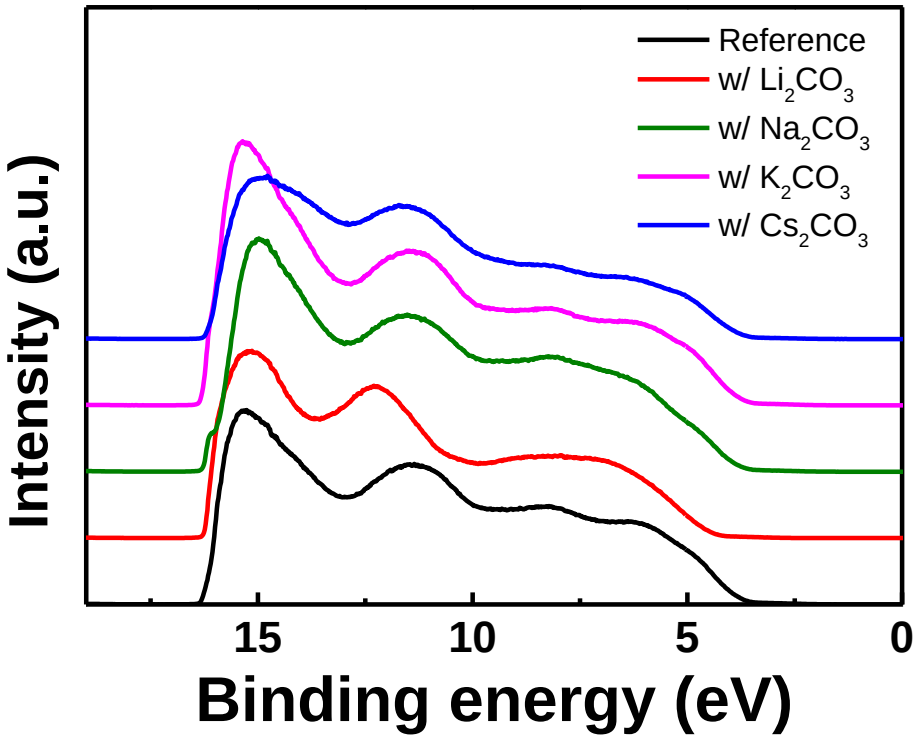

Figure 3.6 Ultra-violet photoelectron spectra (UPS) data of the Pristine ZnO layer and each ZnO doped with metal carbonate layer.

	Valence band (eV)	Work function (eV)
Pristine ZnO	6.82	4.86
w/ Li_2CO_3	7.51	4.95
w/ Na_2CO_3	7.00	5.14
w/ K_2CO_3	6.84	4.88
w/ Cs_2CO_3	7.18	5.04

Table 3.2 Valence Band (E_v) work function of Pristine ZnO and each ZnO doped with metal carbonate layer from UPS measurement

To investigate electrical properties of alkali metal carbonates on ZnO nanoparticle layers, we collected X-ray photoelectron spectra (XPS) and Ultraviolet photoelectron spectra (UPS). **Figure 3.5a** showed the Li 2p photo-emission peak in ZnO doped with Li_2CO_3 layer whereas pristine ZnO has any Li 2p

peak at all. Also, we obtained Na 1s, K 2p and Cs 3d peaks in ZnO doped with Na_2CO_3, K_2CO_3 and Cs_2CO_3 layers as shown in **Figure 3.5.** These results indicate that all alkali metal carbonates influenced the electronic properties of the ZnO nanoparticle layer. We also observed that these doped metal carbonates play a key role to change the energy level of ZnO layer from the UPS analysis (**Figure 3.6**, **Table 3.2**). Secondary cutoff edge which gave the work function level in accordance with gold work function and Fermi edge region which presented the valence band maximum (VBM) of each layer was gathered to identify the Valence band (VB) of doped carbonate series. VB level of the pristine ZnO was much shallow than others, 6.82 eV. ZnO doped with Li_2CO_3 had the deepest VB of 7.19 eV. Other VB levels are 7.00 eV of Na_2CO_3, 6.84 eV of K_2CO_3, and 7.18 eV of Cs_2CO_3.

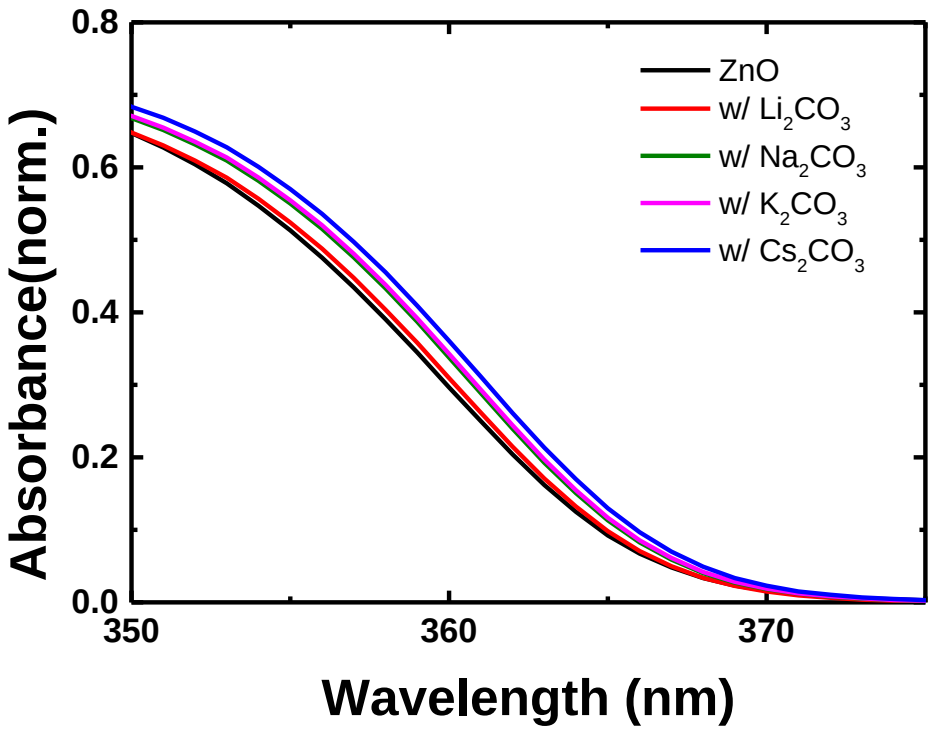

Figure 3.7a UV-Vis absorption spectrum.

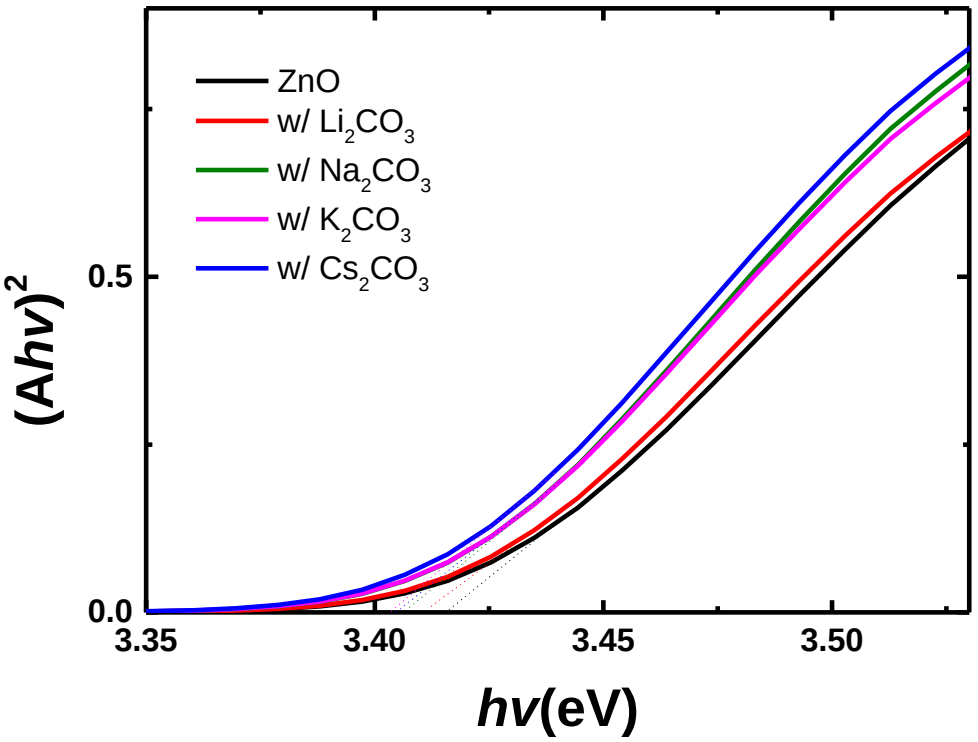

Figure 3.7b tauc plot spectra of pristine ZnO and ZnO treated with various metal carbonates.

	Energy Gap (eV)
Pristine ZnO	3.42
w/ Li_2CO_3	3.41
w/ Na_2CO_3	3.40
w/ K_2CO_3	3.41
w/ Cs_2CO_3	3.40

Table 3.3 Energy gap (E_g) of Pristine ZnO and each ZnO doped with metal carbonate layer derived from Tauc plots

To get the Conduction band (CB) level, we used valence band level from UPS and optical energy band gap from tauc plot (**Figure 3.7, Table 3.3**). Tauc plot was originated from UV-Vis absorption spectrum. Optical band gap of pristine ZnO and all doped ZnO almost same. Using two values, we could get the CB level. Tendency of CB was similar with those of VB.

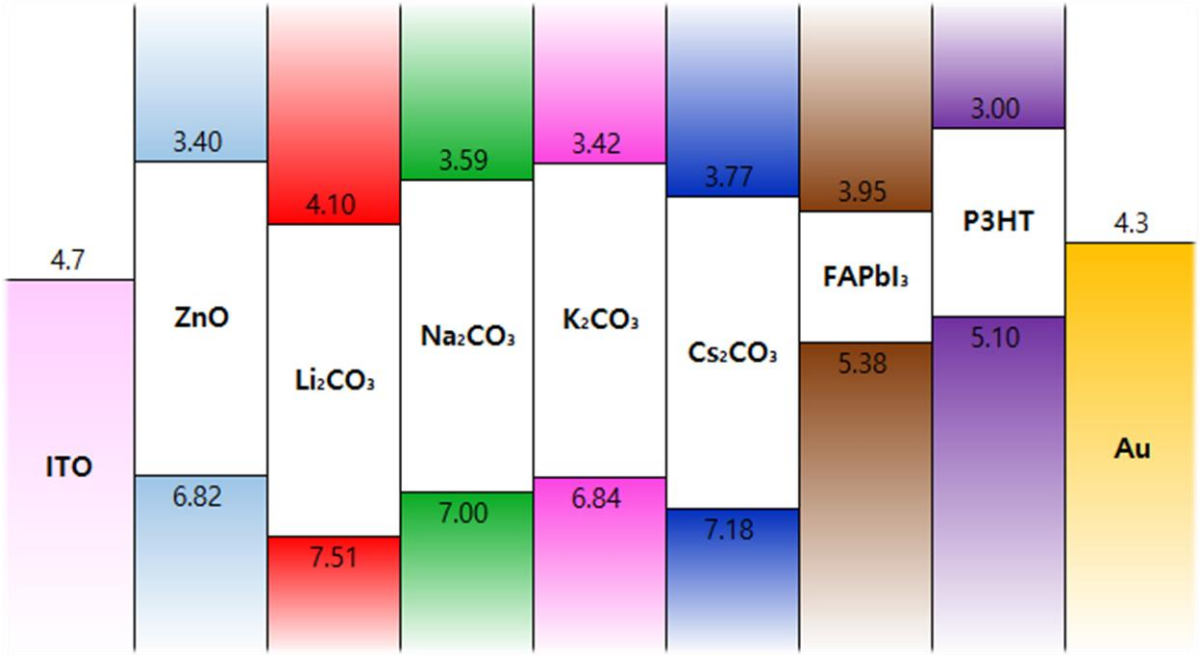

Figure 3.8 Energy band diagram of the ITO/ZnO/M2CO3/FAPbI3/P3HT/Au junction, showing the influence of various alkali metal carbonates on the ETL band structure.

According to **Figure 3.8,** CB of pristine ZnO was the highest among them, 3.40 eV. Compared to pristine ZnO, VB level of ZnO doped with Cs_2CO_3 was highly changed. Then CB level was 3.77 eV. Also, VB level of ZnO doped with Li_2CO_3 was changed dramatically, so CB level was 4.10 eV. That means electrons could be more freely transferred to ZnO doped with metal carbonate layer than pristine ZnO from perovskite layer due to lower energy barrier. Then it was expected that lower energy barrier affect to PCE. Although doping material make energy level of each layer changed, morphology of the ZnO layers doped with various carbonate looked similar.

3.4 Analysis of morphology

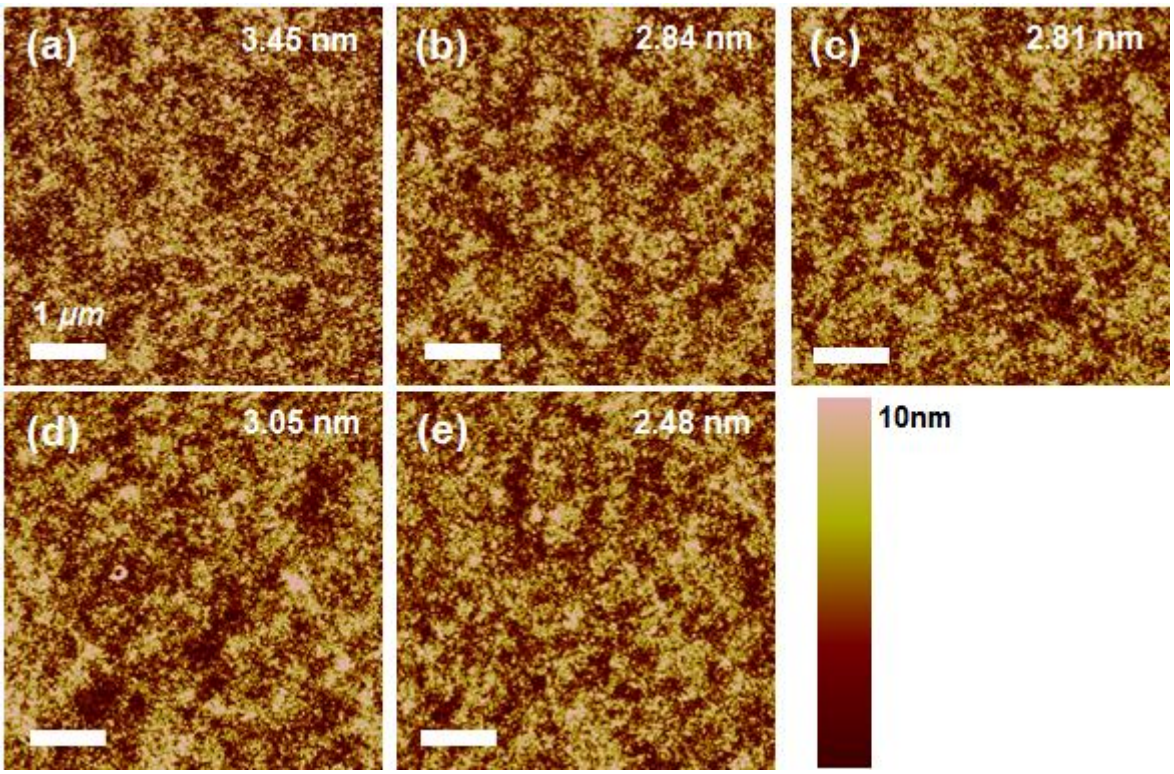

Figure 3.9 AFM height images (10 μm * 10 μm) of (a) pristine ZnO nanoparticle layer (b) Li_2CO_3 deposited on the ZnO layer (c) Na_2CO_3 deposited on the ZnO layer (d) K_2CO_3 deposited on the ZnO layer (e) Cs_2CO_3 deposited on the ZnO layer.

Figure 3.9 shows atomic force microscopy (AFM) images of pristine ZnO and metal carbonate solution on ZnO. RMS values were found to be 2.84 nm for ZnO with Li_2CO_3, 2.81 nm for ZnO with Na_2CO_3, 3.05 nm for ZnO with K_2CO_3, and 2.48 nm for ZnO with Cs_2CO_3.

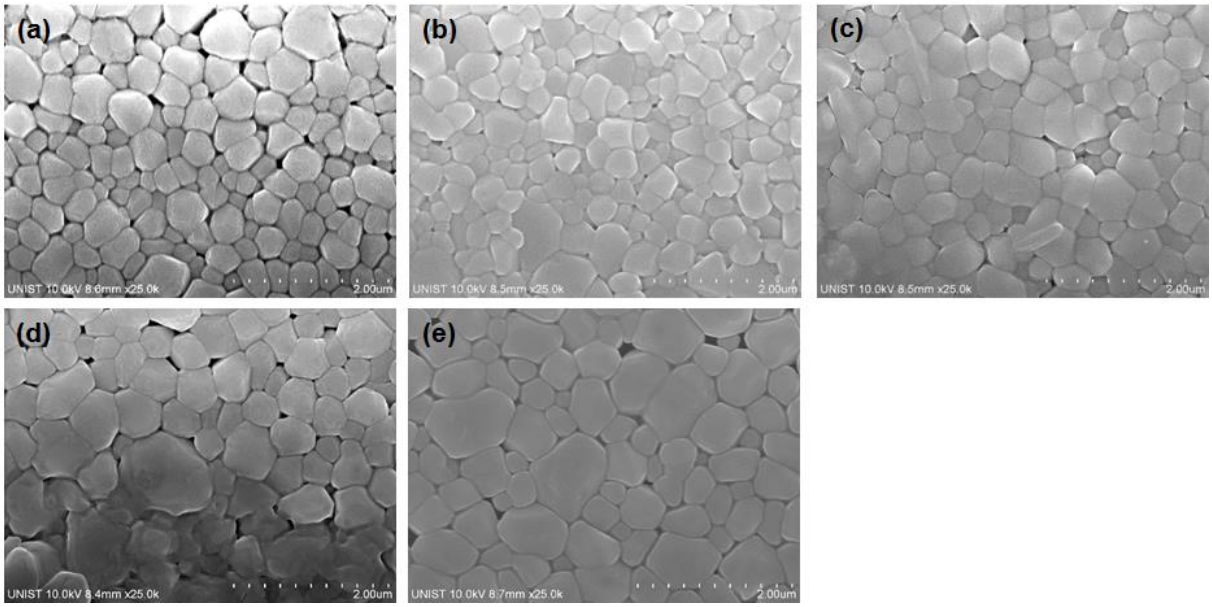

Figure 3.10 SEM top-view images of FAPbI3 deposited on (a) a pristine ZnO nanoparticle layer, (b) ZnO doped with Li_2CO_3, (c) ZnO doped with Na_2CO_3, (d) ZnO doped with K_2CO_3 and (e) ZnO doped with Cs_2CO_3.

After that, we checked the morphology of the $FAPbI_3$ layer deposited on pristine ZnO, and various metal doped ZnO via morphology images of SEM in **Figure 3.10**. The device using K doped ZnO and Cs doped ZnO had larger grain size than pristine ZnO. And grain shape looks similar.

3.5 Result and discussion

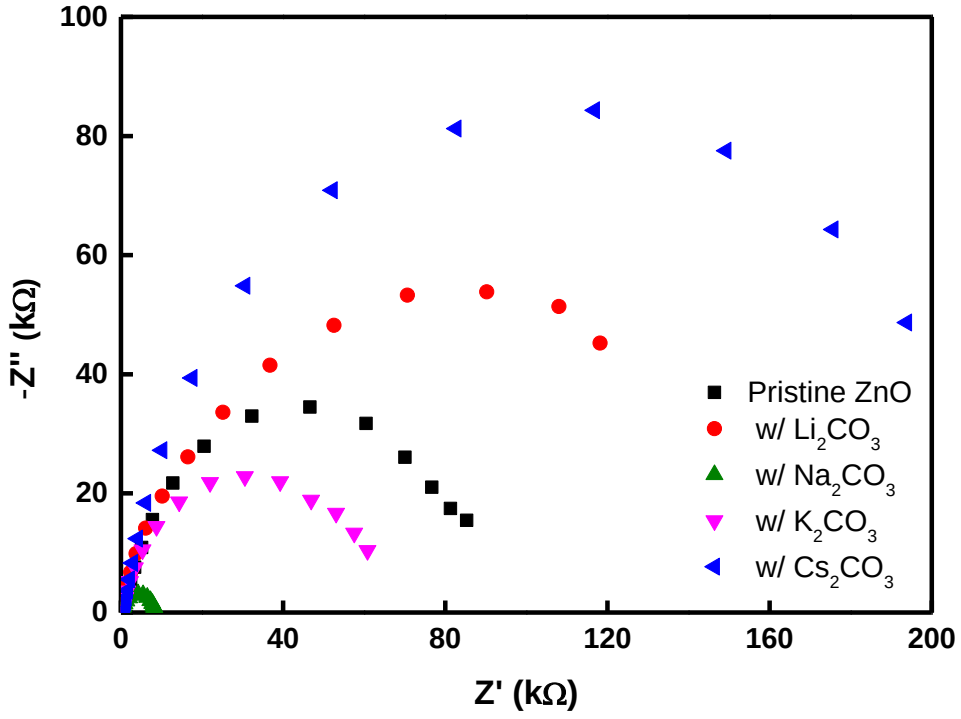

Figure 3.11 Electrochemical impedance spectra (Nyquist plot) of perovskite solar cells with and without a doped ZnO.

Addition to improvement of the ZnO layer using alkali metal carbonates, we made the full device cell. To get further information about the interfacial properties, we check the Electrochemical impedance spectrum (EIS) in **Figure 3.11**. This result is different with tendency of the energy level diagram. EIS was conducted to study about the alkali metal-doped ZnO effect. It can be measured the interfacial properties, such as recombination and electron transport. Nyquist plots of the EIS are measured under dark conditions at 0 V. All plots have one semicircle without transmission line (TL) behavior.[95] The absence of the TL patterns indicated that the recombination of the solar cell is strong interpreted by the Gerischer impedance model. Further, single semicircle indicates that interface contact between the perovskite layer and the ZnO layer are not likely to be rectifying contacts. In addition, Semicircle size is related to the amount of the recombination resistance. That means, the device with ZnO doped with Cs_2CO_3 has higher recombination resistance than with ZnO doped with Li_2CO_3. Except for doping process, all device fabrication parameters were identical. After all, doping only induced the recombination resistance. As recombination resistance is higher (lower recombination rates), the solar cell performance was increased.

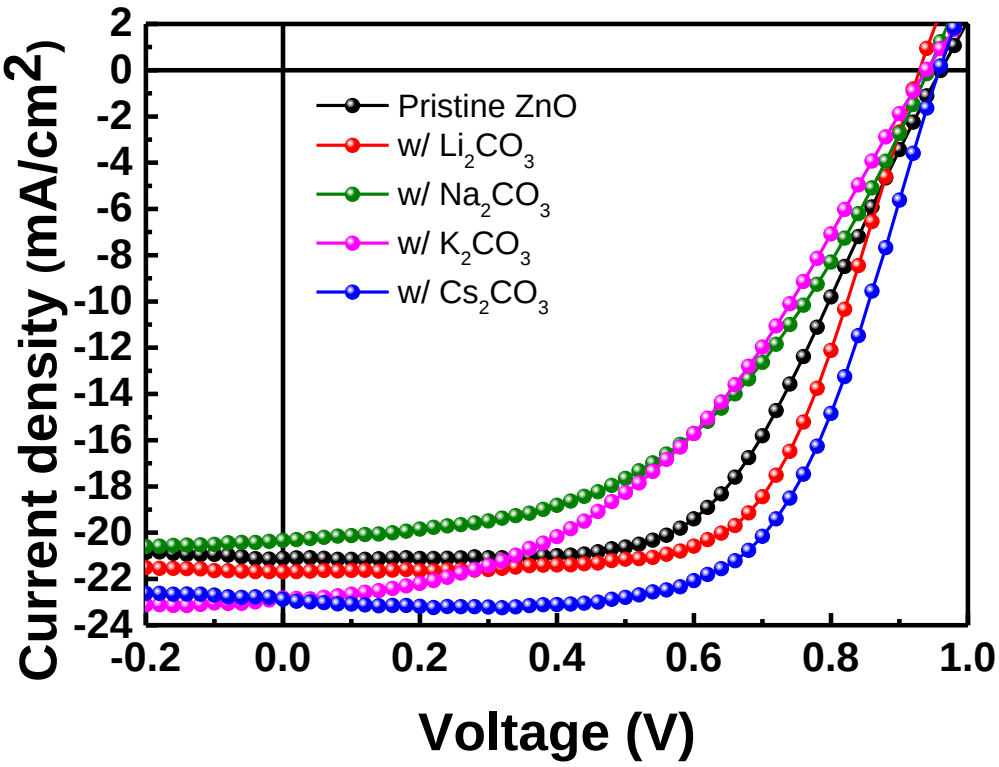

Figure 3.12 Current density – voltage characteristics of $FAPbI_3$ planar solar cells deposited on the pristine ZnO layer and each ZnO doped with metal carbonate under 100mW cm^{-2} AM1.5 illumination.

Doped metal carbonate	J_{SC} (mA/cm²)	V_{OC} (V)	*FF*	PCE (%)	Cal. J_{SC} (mA/cm²)
Pristine ZnO	21.1	0.96	0.58	11.7	19.7
w/ Li_2CO_3	21.7	0.93	0.65	13.0	21.4
w/ Na_2CO_3	20.3	0.94	0.49	9.43	20.3
w/ K_2CO_3	22.8	0.94	0.44	9.45	21.9
w/ Cs_2CO_3	23.1	0.98	0.62	14.1	21.8

Table 3.4 Solar cell characteristic of $FAPbI_3$ deposited on pristine ZnO and ZnO doped with various metal carbonates.

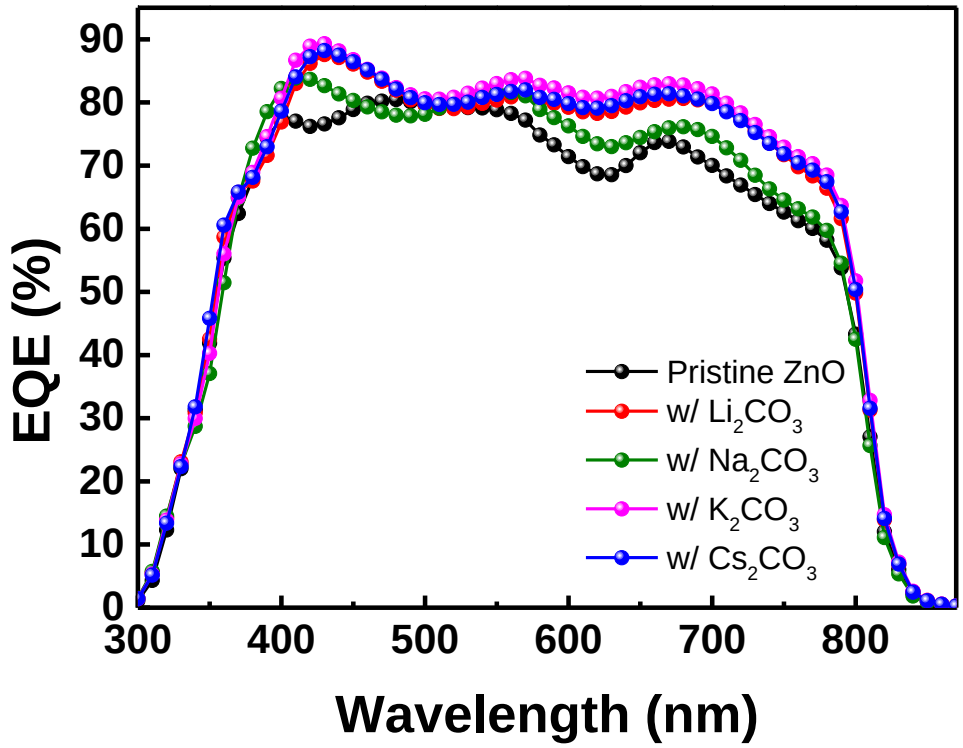

Figure 3.13 External Quantum Efficiency spectra of $FAPbI_3$ planar solar cells deposited on the pristine ZnO layer and each ZnO doped with metal carbonate.

Figure 3.12 shows current density - voltage curve of $FAPbI_3$ layer deposited on the pristine ZnO or other ZnO doped with various alkali metal carbonate. With Pristine ZnO, the device yielded PCE of 11.7%. It had J_{sc} of 21.1 mA cm^{-2}, V_{oc} of 0.96 V and FF of 0.58. Li_2CO_3 and Cs_2CO_3 made ZnO energy level down, then make the energy barrier also low. So, FF and J_{sc} of two devices for ZnO doped with Li_2CO_3 and with Cs_2CO_3 were enhanced. Among them, the device doped with Cs_2CO_3 had 23.1 mA cm^{-2}, 0.98 V and FF of 0.62. So, this device had highest efficiency of 14.1%. In the device doped with Li_2CO_3 case, it had J_{sc} of 21.7 mA cm^{-2}, V_{oc} of 0.93 V, FF of 0.65 and PCE of 13.0%. Other details related to each cell performance of these solar cells are listed in **Table 3.4**. This tendency of the efficiency is similar with that of recombination resistance. **Figure 3.13** shows EQE curve. Spectrum shape of the device used ZnO doped with alkali metal carbonate looks little different with used pristine ZnO.

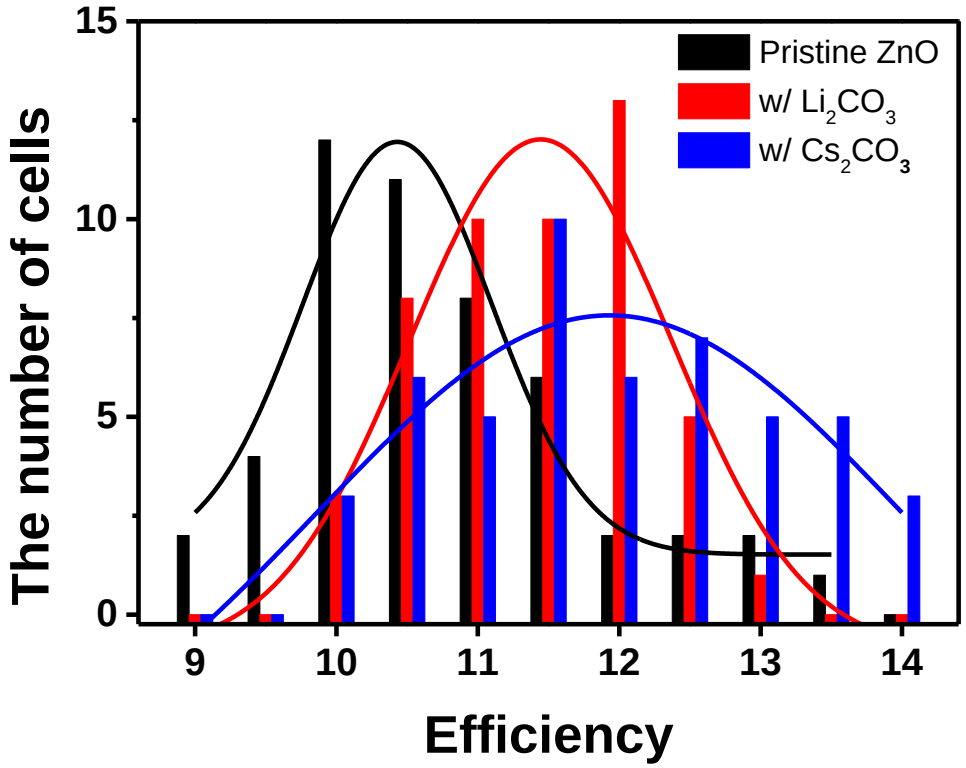

Figure 3.14 Histogram and Gaussian curves of the device efficiency about $FAPbI_3$ perovskite solar cell deposited on the pristine ZnO, ZnO doped with Li_2CO_3, and ZnO doped with Cs_2CO_3.

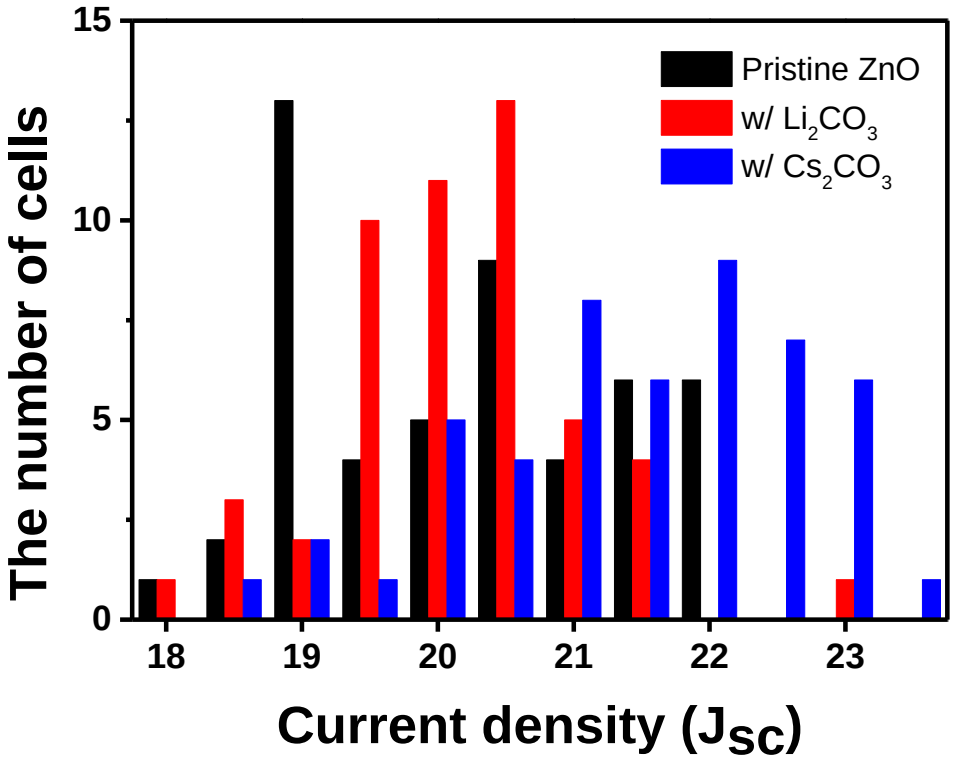

Figure 3.15 Histogram of the device short circuit current density about $FAPbI_3$ perovskite solar cell deposited on the pristine ZnO, ZnO doped with Li_2CO_3, and ZnO doped with Cs_2CO_3.

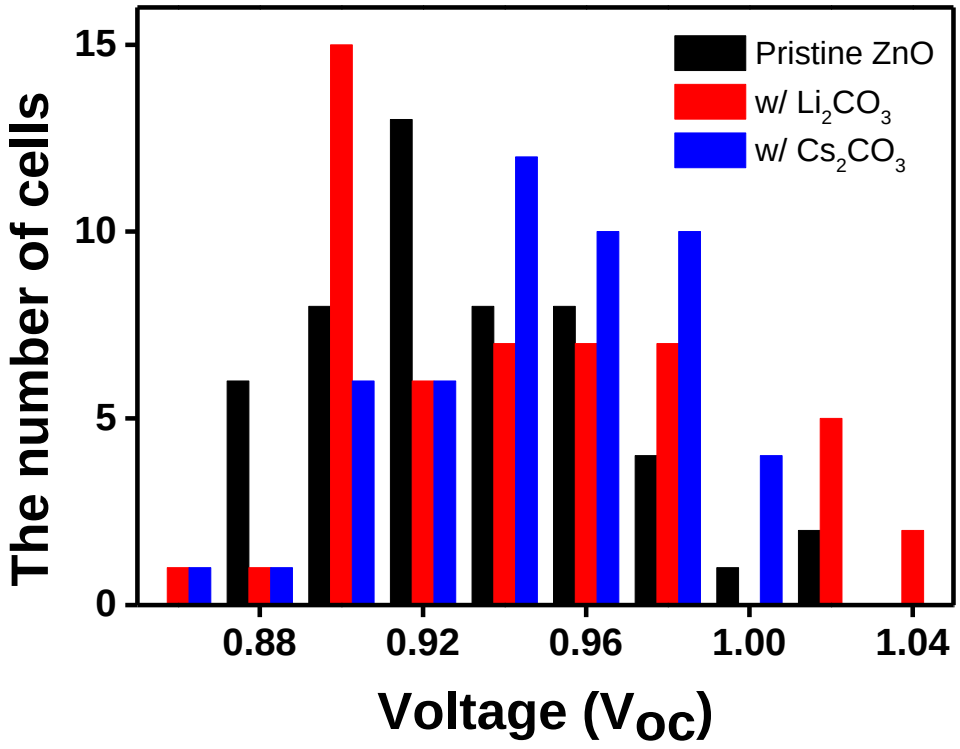

Figure 3.16 Histogram of the device open circuit voltage about $FAPbI_3$ perovskite solar cell deposited on the pristine ZnO, ZnO doped with Li_2CO_3, and ZnO doped with Cs_2CO_3.

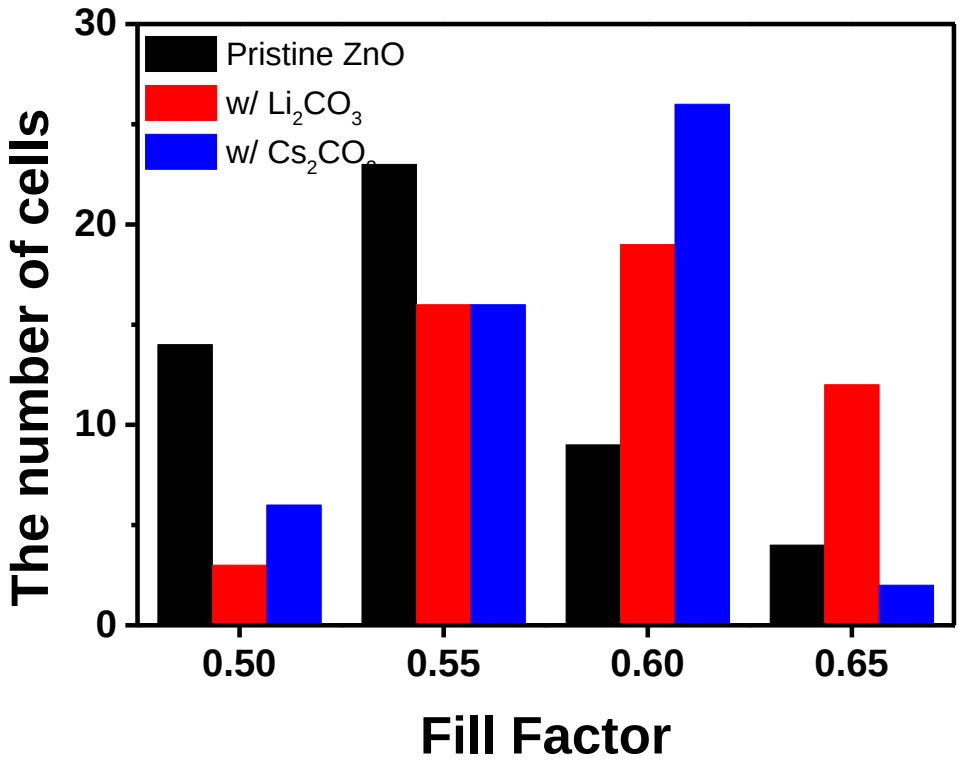

Figure 3.17 Histogram of the device fill factor about $FAPbI_3$ perovskite solar cell deposited on the pristine ZnO, ZnO doped with Li_2CO_3, and ZnO doped with Cs_2CO_3.

Figure 3.14 shows PCE statistics for solar cells using $FAPbI_3$ layers deposited on pristine ZnO, ZnO doped with Li_2CO_3 and ZnO doped with Cs_2CO_3, while statistics for individual device parameters are reported. This curve shows that devices using ZnO doped with Cs_2CO_3 yielded significantly higher J_{sc} compared to other devices which used pristine ZnO, or ZnO doped with Li_2CO_3. To demonstrate the accuracy of tendency, we made the histograms of J_{sc}, V_{oc}, and FF for 50 individual devices for $FAPbI_3$ perovskite solar cell using the pristine ZnO, Li-doped ZnO, Cs-doped ZnO. In **Figure 3.15**, average of J_{sc} was increased per pristine ZnO, Li-doped ZnO, Cs-doped ZnO. V_{oc} average was approximately similar in **Figure 3.16**. In case of FF, the device using doped ZnO has higher value than using pristine ZnO due to lower energy barrier (**Figure 3.17**).

3.6 Conclusion

In summary, I successfully investigated $FAPbI_3$ perovskite solar cells using doped alkali carbonate including Li_2CO_3, Na_2CO_3, K_2CO_3 and Cs_2CO_3 on ZnO ETL with low temperature solution processing techniques. As an alternative to TiO_2, ZnO nanoparticles are electron transport materials for efficient n-i-p planar heterojunction solar cells which can be used on flexible substrate via roll-to-roll processing. Due to base characteristic of ZnO, I optimized the uniform and dense $FAPbI_3$ layer on ZnO. But there is energy barrier between conduction band of ZnO and that of $FAPbI_3$. To solve this problem, I focused the tuning the energy band. These alkali carbonate is well modified the CB level of ZnO. Doped ZnO lead electrons easily transport from perovskite to cathode electrode. Additionally, perovskite solar cells with Cs-doped ZnO have lower recombination rates than solar cells with other doped ZnO or pristine ZnO. Thus, the perovskite solar cell using Cs-doped ZnO showed higher performance than those of other alkali metal carbonate over 14.1% PCE.

3.7 Experiment method

All chemicals were purchased from Sigma Aldrich and used as received.

Preparation of ZnO nanoparticle: ZnO nanoparticles were prepared by reaction between a zinc acetate solution (23.6 mg ml^{-1} [$Zn(CH_3COO)_2.2H_2O$] in methanol) and a potassium hydroxide solution (31.6 mg ml^{-1} in metanol in a 250 mL round bottom flask at 60 ^oC for 21 h with string. And then this particle was dissolved in CF, Methanol mixture.[96]

*Preparation of the perovskite precursor***:** MAI was prepared by reacting 30 ml of methylamine solution (40 % in water) with 30 ml of hydroiodic acid (57 wt% in water) in 250 ml round bottom flask at 0 ^oC for 2 h under string with the Argon condition. And the solvent was thermal evaporated under vacuum at 60 ^oC for 1 h to obtain a white raw product. The white raw product was washed with diethyl ether three times. After filtration, the product was dissolved in ethanol and recrystallized by ethanol for 20 h. Then the precipitate was washed with diethyl ether and filtered. The filtered solid was dried at 60 ^oC under vacuum for 24 h. FAI was prepared by reacting 0.45 g ml^{-1} solution of formamidinium acetate in absolute methanol with 30 ml of HI. The reaction conditions and cleaning process were same to those of MAI preparation. To prepare perovskite precursors, Firstly PbI_2 was dissolved in DMF for a concentration of 1.3 M with NMP 1 mM and secondly FAI(MAI) was dissolved in isopropanol of 80 mg $ml^{-}1$(65 mg ml^{-1}). This obtained solution was stirred at room temperature for 1 h in air and used subsequently for device fabrication.

Device fabrication and characterization: ITO-coated glass substrates were washed by ultrasonication

with DI water, acetone, and isopropanol for 20 minutes each. ZnO nanoparticles were spin coated at 3000 rpm for 10 s. For the perovskite layer, PbI_2 was dissolved in DMF and spin coated at 5000 rpm for 30 s. Secondly 80 mg ml^{-1} FAI in isopropanol was dropped on the PbI_2 film and spin coated at 5000 rpm for 30 s and dried at 130 ^oC for 20 min. MAI are similar to FAI, apart from concentration and annealing condition, which was 65 mg ml^{-1}, and 100 ^oC for 2 min. During that process, perovskite film was formed. 20 mg ml^{-1} P3HT dissolved in CB were deposited on the perovskite layer by spin coating at 1000 rpm for 30 s. In that case, P3HT solution didn't contain any dopant like Li-TFSI or TBP. Finally, 70 nm gold was deposited by thermal evaporating under vacuum ($<10^{-6}$ Torr).

The current density-voltage (J-V) characterization of the solar cell devices were obtained using a Kiethley 2635A Source Measure Unit under AM1.5G with irradiation intensity of 100 mW cm^{-1}. The active layer was 0.13 cm^2. External Quantum Efficiency (EQE) measurements were measured with a PV measurement QE system under ambient conditions. With monochromated light from a xenon arc lamp.

Film characterization: Scanning electron microscope measurements (SEM) were performed using an S-4800 Hitachi high-Technology microscope. SEM samples were prepared by deposited perovskite precursor solutions on ZnO or doped ZnO layer by spin-coating two step method, followed by annealing at 130 ℃ for 10 min on a hotplate. UV-vis absorption was measured using a Varian Cary 5000 spectrophotometer. AFM images were obtained using a Veeco Multimode AFM microscope in a tapping mode.

References

1. Becquerel, A., Mémoire sur les effets électriques produits sous l'influence des rayons solaires. Comptes Rendus 9: 561–567. *Originalarbeit zur Einwirkung von Licht auf Elektroden* **1839**.

2. Adams, W. G.; Day, R., The Action of Light on Selenium. *Proceedings of the Royal Society of London* **1876,** *25* (171-178), 113-117.

3. Pochettino, A., Sul comportamento foto-elettrico dell'antracene. *Acad. Lincei Rend* **1906,** *15*, 355.

4. Chapin, D. M.; Fuller, C.; Pearson, G., A new silicon p-n junction photocell for converting solar radiation into electrical power. *Journal of Applied Physics* **1954,** *25* (5), 676-677.

5. Shirakawa, H.; Louis, E. J.; MacDiarmid, A. G.; Chiang, C. K.; Heeger, A. J., Synthesis of electrically conducting organic polymers: halogen derivatives of polyacetylene,(CH) x. *Journal of the Chemical Society, Chemical Communications* **1977,** (16), 578-580.

6. Kojima, A.; Teshima, K.; Shirai, Y.; Miyasaka, T., Organometal halide perovskites as visible-light sensitizers for photovoltaic cells. *Journal of the American Chemical Society* **2009,** *131* (17), 6050-6051.

7. Pena, M.; Fierro, J., Chemical structures and performance of perovskite oxides. *Chemical reviews* **2001,** *101* (7), 1981-2018.

8. Goldschmidt, V., Krystallbau und chemische Zusammensetzung. *Berichte der deutschen chemischen Gesellschaft (A and B Series)* **1927,** *60* (5), 1263-1296.

9. Chen, F., Optically induced change of refractive indices in LiNbO3 and LiTaO3. *Journal of applied physics* **1969,** *40* (8), 3389-3396.

10. Cao, D.; Wang, C.; Zheng, F.; Dong, W.; Fang, L.; Shen, M., High-efficiency ferroelectric-film solar cells with an n-type Cu2O cathode buffer layer. *Nano letters* **2012,** *12* (6), 2803-2809.

11. Salau, A., Fundamental absorption edge in PbI2: KI alloys. *Solar Energy Materials* **1980,** *2* (3), 327-332.

12. Burroughes, J.; Bradley, D.; Brown, A.; Marks, R.; Mackay, K.; Friend, R.; Burns, P.; Holmes, A., Light-emitting diodes based on conjugated polymers. *nature* **1990,** *347* (6293), 539-541.

13. Kagan, C.; Mitzi, D.; Dimitrakopoulos, C., Organic-inorganic hybrid materials as semiconducting channels in thin-film field-effect transistors. *Science* **1999,** *286* (5441), 945-947.

14. Im, J.-H.; Lee, C.-R.; Lee, J.-W.; Park, S.-W.; Park, N.-G., 6.5% efficient perovskite quantum-dot-sensitized solar cell. *Nanoscale* **2011,** *3* (10), 4088-4093.

15. Kim, H.-S.; Lee, C.-R.; Im, J.-H.; Lee, K.-B.; Moehl, T.; Marchioro, A.; Moon, S.-J.; Humphry-Baker, R.; Yum, J.-H.; Moser, J. E., Lead iodide perovskite sensitized all-solid-state submicron thin film mesoscopic solar cell with efficiency exceeding 9%. *Scientific reports* **2012,** *2*, 591.

16. Lee, M. M.; Teuscher, J.; Miyasaka, T.; Murakami, T. N.; Snaith, H. J., Efficient hybrid solar cells based on meso-superstructured organometal halide perovskites. *Science* **2012,** *338* (6107), 643-647.

17. Borriello, I.; Cantele, G.; Ninno, D., Ab initio investigation of hybrid organic-inorganic perovskites based on tin halides. *Physical Review B* **2008,** *77* (23), 235214.

18. Noh, J. H.; Im, S. H.; Heo, J. H.; Mandal, T. N.; Seok, S. I., Chemical management for colorful, efficient, and stable inorganic–organic hybrid nanostructured solar cells. *Nano letters* **2013,** *13* (4), 1764-1769.

19. Kulkarni, S. A.; Baikie, T.; Boix, P. P.; Yantara, N.; Mathews, N.; Mhaisalkar, S., Band-gap tuning of lead halide perovskites using a sequential deposition process. *Journal of Materials Chemistry A* **2014,** *2* (24), 9221-9225.

20. Eperon, G. E.; Stranks, S. D.; Menelaou, C.; Johnston, M. B.; Herz, L. M.; Snaith, H. J., Formamidinium lead trihalide: a broadly tunable perovskite for efficient planar heterojunction solar cells. *Energy & Environmental Science* **2014,** *7* (3), 982-988.

21. McKinnon, N. K.; Reeves, D. C.; Akabas, M. H., 5-HT3 receptor ion size selectivity is a property of the transmembrane channel, not the cytoplasmic vestibule portals. *The Journal of general physiology* **2011,** *138* (4), 453-466.

22. Pang, S.; Hu, H.; Zhang, J.; Lv, S.; Yu, Y.; Wei, F.; Qin, T.; Xu, H.; Liu, Z.; Cui, G., NH2CH□NH2PbI3: An Alternative Organolead Iodide Perovskite Sensitizer for Mesoscopic Solar Cells. *Chemistry of Materials* **2014,** *26* (3), 1485-1491.

23. Miller, O. D.; Yablonovitch, E.; Kurtz, S. R., Strong internal and external luminescence as solar cells approach the Shockley–Queisser limit. *IEEE Journal of Photovoltaics* **2012,** *2* (3), 303-311.

24. Im, J.-H.; Chung, J.; Kim, S.-J.; Park, N.-G., Synthesis, structure, and photovoltaic property of a nanocrystalline 2H perovskite-type novel sensitizer (CH 3 CH 2 NH 3) PbI 3. *Nanoscale research letters* **2012,** *7* (1), 1.

25. Burschka, J.; Pellet, N.; Moon, S.-J.; Humphry-Baker, R.; Gao, P.; Nazeeruddin, M. K.; Grätzel, M., Sequential deposition as a route to high-performance perovskite-sensitized solar cells. *Nature* **2013,** *499* (7458), 316-319.

26. Koh, T. M.; Fu, K.; Fang, Y.; Chen, S.; Sum, T.; Mathews, N.; Mhaisalkar, S. G.; Boix, P. P.; Baikie, T., Formamidinium-containing metal-halide: An alternative material for near-IR absorption perovskite solar cells. *The Journal of Physical Chemistry C* **2013,** *118* (30), 16458-16462.

27. Umari, P.; Mosconi, E.; De Angelis, F., Relativistic GW calculations on CH3NH3PbI3 and CH3NH3SnI3 perovskites for solar cell applications. *Scientific reports* **2014,** *4*.

28. Hao, F.; Stoumpos, C. C.; Cao, D. H.; Chang, R. P.; Kanatzidis, M. G., Lead-free solid-state organic-inorganic halide perovskite solar cells. *Nature Photonics* **2014,** *8* (6), 489-494.

29. Bernal, C.; Yang, K., First-Principles Hybrid Functional Study of the Organic–Inorganic Perovskites CH3NH3SnBr3 and CH3NH3SnI3. *The Journal of Physical Chemistry C* **2014,** *118* (42), 24383-24388.

30. Knutson, J. L.; Martin, J. D.; Mitzi, D. B., Tuning the band gap in hybrid tin iodide perovskite semiconductors using structural templating. *Inorganic chemistry* **2005,** *44* (13), 4699-4705.

31. Stoumpos, C. C.; Malliakas, C. D.; Kanatzidis, M. G., Semiconducting tin and lead iodide perovskites with organic cations: phase transitions, high mobilities, and near-infrared photoluminescent properties. *Inorganic chemistry* **2013,** *52* (15), 9019-9038.

32. Ogomi, Y.; Morita, A.; Tsukamoto, S.; Saitho, T.; Fujikawa, N.; Shen, Q.; Toyoda, T.; Yoshino, K.; Pandey, S. S.; Ma, T., CH3NH3Sn x Pb (1–x) I3 Perovskite solar cells covering up to 1060 nm. *The journal of physical chemistry letters* **2014,** *5* (6), 1004-1011.

33. Mosconi, E.; Amat, A.; Nazeeruddin, M. K.; Grätzel, M.; De Angelis, F., First-principles modeling of mixed halide organometal perovskites for photovoltaic applications. *The Journal of Physical Chemistry C* **2013,** *117* (27), 13902-13913.

34. Jiang, M.; Wu, J.; Lan, F.; Tao, Q.; Gao, D.; Li, G., Enhancing the performance of planar organo-lead halide perovskite solar cells by using a mixed halide source. *Journal of Materials Chemistry A* **2015,** *3* (3), 963-967.

35. Stranks, S. D.; Eperon, G. E.; Grancini, G.; Menelaou, C.; Alcocer, M. J.; Leijtens, T.; Herz, L. M.; Petrozza, A.; Snaith, H. J., Electron-hole diffusion lengths exceeding 1 micrometer in an organometal trihalide perovskite absorber. *Science* **2013,** *342* (6156), 341-344.

36. Niu, G.; Guo, X.; Wang, L., Review of recent progress in chemical stability of perovskite solar cells. *Journal of Materials Chemistry A* **2015,** *3* (17), 8970-8980.

37. Chung, I.; Lee, B.; He, J.; Chang, R. P.; Kanatzidis, M. G., All-solid-state dye-sensitized solar cells with high efficiency. *Nature* **2012,** *485* (7399), 486-489.

38. Nagane, S.; Bansode, U.; Game, O.; Chhatre, S.; Ogale, S., CH 3 NH 3 PbI (3− x)(BF 4) x: molecular ion substituted hybrid perovskite. *Chemical Communications* **2014,** *50* (68), 9741-9744.

39. Park, N.-G., Organometal perovskite light absorbers toward a 20% efficiency low-cost solid-state mesoscopic solar cell. *The Journal of Physical Chemistry Letters* **2013,** *4* (15), 2423-2429.

40. Qiu, J.; Qiu, Y.; Yan, K.; Zhong, M.; Mu, C.; Yan, H.; Yang, S., All-solid-state hybrid solar cells based on a new organometal halide perovskite sensitizer and one-dimensional TiO 2 nanowire arrays. *Nanoscale* **2013,** *5* (8), 3245-3248.

41. Zhang, X.; Bao, Z.; Tao, X.; Sun, H.; Chen, W.; Zhou, X., Sn-doped TiO 2 nanorod arrays and application in perovskite solar cells. *RSC Advances* **2014,** *4* (109), 64001-64005.

42. Kim, H.-S.; Lee, J.-W.; Yantara, N.; Boix, P. P.; Kulkarni, S. A.; Mhaisalkar, S.; Grätzel, M.; Park, N.-G., High efficiency solid-state sensitized solar cell-based on submicrometer rutile TiO2 nanorod and CH3NH3PbI3 perovskite sensitizer. *Nano letters* **2013,** *13* (6), 2412-2417.

43. Gao, X.; Li, J.; Baker, J.; Hou, Y.; Guan, D.; Chen, J.; Yuan, C., Enhanced photovoltaic performance of perovskite CH 3 NH 3 PbI 3 solar cells with freestanding TiO 2 nanotube array films. *Chemical Communications* **2014,** *50* (48), 6368-6371.

44. Zhong, D.; Cai, B.; Wang, X.; Yang, Z.; Xing, Y.; Miao, S.; Zhang, W.-H.; Li, C., Synthesis of oriented TiO 2 nanocones with fast charge transfer for perovskite solar cells. *Nano Energy* **2015,** *11*, 409-418.

45. Etgar, L.; Gao, P.; Xue, Z.; Peng, Q.; Chandiran, A. K.; Liu, B.; Nazeeruddin, M. K.; Grätzel, M., Mesoscopic CH3NH3PbI3/TiO2 heterojunction solar cells. *Journal of the American Chemical Society* **2012,** *134* (42), 17396-17399.

46. Mei, A.; Li, X.; Liu, L.; Ku, Z.; Liu, T.; Rong, Y.; Xu, M.; Hu, M.; Chen, J.; Yang, Y., A hole-conductor–free, fully printable mesoscopic perovskite solar cell with high stability. *Science* **2014,** *345* (6194), 295-298.

47. Chen, Q.; De Marco, N.; Yang, Y. M.; Song, T.-B.; Chen, C.-C.; Zhao, H.; Hong, Z.; Zhou, H.; Yang, Y., Under the spotlight: The organic–inorganic hybrid halide perovskite for optoelectronic applications. *Nano Today* **2015,** *10* (3), 355-396.

48. Snaith, H. J.; Grätzel, M., Electron and Hole Transport through Mesoporous TiO2 Infiltrated with Spiro□MeOTAD. *Advanced Materials* **2007,** *19* (21), 3643-3647.

49. Cappel, U. B.; Daeneke, T.; Bach, U., Oxygen-induced doping of spiro-MeOTAD in solid-state dye-sensitized solar cells and its impact on device performance. *Nano letters* **2012,** *12* (9), 4925-4931.

50. Qin, P.; Tanaka, S.; Ito, S.; Tetreault, N.; Manabe, K.; Nishino, H.; Nazeeruddin, M. K.; Grätzel, M., Inorganic hole conductor-based lead halide perovskite solar cells with 12.4% conversion efficiency. *Nature communications* **2014,** *5*.

51. Zheng, L.; Chung, Y.-H.; Ma, Y.; Zhang, L.; Xiao, L.; Chen, Z.; Wang, S.; Qu, B.; Gong, Q., A

hydrophobic hole transporting oligothiophene for planar perovskite solar cells with improved stability. *Chemical Communications* **2014,** *50* (76), 11196-11199.

52. Cheng, M.; Xu, B.; Chen, C.; Yang, X.; Zhang, F.; Tan, Q.; Hua, Y.; Kloo, L.; Sun, L., Phenoxazine□ Based Small Molecule Material for Efficient Perovskite Solar Cells and Bulk Heterojunction Organic Solar Cells. *Advanced Energy Materials* **2015,** *5* (8).

53. Heo, J. H.; Im, S. H.; Noh, J. H.; Mandal, T. N.; Lim, C.-S.; Chang, J. A.; Lee, Y. H.; Kim, H.-j.; Sarkar, A.; Nazeeruddin, M. K., Efficient inorganic-organic hybrid heterojunction solar cells containing perovskite compound and polymeric hole conductors. *Nature Photonics* **2013,** *7* (6), 486-491.

54. Habisreutinger, S. N.; Leijtens, T.; Eperon, G. E.; Stranks, S. D.; Nicholas, R. J.; Snaith, H. J., Carbon nanotube/polymer composites as a highly stable hole collection layer in perovskite solar cells. *Nano letters* **2014,** *14* (10), 5561-5568.

55. Christians, J. A.; Fung, R. C.; Kamat, P. V., An inorganic hole conductor for organo-lead halide perovskite solar cells. Improved hole conductivity with copper iodide. *Journal of the American Chemical Society* **2013,** *136* (2), 758-764.

56. Wang, K.-C.; Jeng, J.-Y.; Shen, P.-S.; Chang, Y.-C.; Diau, E. W.-G.; Tsai, C.-H.; Chao, T.-Y.; Hsu, H.-C.; Lin, P.-Y.; Chen, P., p-Type mesoscopic nickel oxide/organometallic perovskite heterojunction solar cells. *Scientific reports* **2014,** *4*.

57. Subbiah, A. S.; Halder, A.; Ghosh, S.; Mahuli, N.; Hodes, G.; Sarkar, S. K., Inorganic hole conducting layers for perovskite-based solar cells. *The journal of physical chemistry letters* **2014,** *5* (10), 1748-1753.

58. Ito, S.; Tanaka, S.; Vahlman, H.; Nishino, H.; Manabe, K.; Lund, P., Carbon□Double□Bond□Free Printed Solar Cells from TiO2/CH3NH3PbI3/CuSCN/Au: Structural Control and Photoaging Effects. *ChemPhysChem* **2014,** *15* (6), 1194-1200.

59. Docampo, P.; Ball, J. M.; Darwich, M.; Eperon, G. E.; Snaith, H. J., Efficient organometal trihalide perovskite planar-heterojunction solar cells on flexible polymer substrates. *Nature communications* **2013,** *4*.

60. Liang, L.; Huang, Z.; Cai, L.; Chen, W.; Wang, B.; Chen, K.; Bai, H.; Tian, Q.; Fan, B., Magnetron sputtered zinc oxide nanorods as thickness-insensitive cathode interlayer for perovskite planar-heterojunction solar cells. *ACS applied materials & interfaces* **2014,** *6* (23), 20585-20589.

61. Jeng, J. Y.; Chiang, Y. F.; Lee, M. H.; Peng, S. R.; Guo, T. F.; Chen, P.; Wen, T. C., CH3NH3PbI3 Perovskite/Fullerene Planar Heterojunction Hybrid Solar Cells. *Advanced Materials* **2013,** *25* (27), 3727-3732.

62. Xiao, Z.; Bi, C.; Shao, Y.; Dong, Q.; Wang, Q.; Yuan, Y.; Wang, C.; Gao, Y.; Huang, J., Efficient, high yield perovskite photovoltaic devices grown by interdiffusion of solution-processed precursor stacking layers. *Energy & Environmental Science* **2014,** *7* (8), 2619-2623.

63. Liu, M.; Johnston, M. B.; Snaith, H. J., Efficient planar heterojunction perovskite solar cells by vapour deposition. *Nature* **2013,** *501* (7467), 395-398.

64. Chen, C. W.; Kang, H. W.; Hsiao, S. Y.; Yang, P. F.; Chiang, K. M.; Lin, H. W., Efficient and uniform planar type perovskite solar cells by simple sequential vacuum deposition. *Advanced Materials* **2014,** *26* (38), 6647-6652.

65. Sutherland, B. R.; Hoogland, S.; Adachi, M. M.; Kanjanaboos, P.; Wong, C. T.; McDowell, J. J.; Xu, J.; Voznyy, O.; Ning, Z.; Houtepen, A. J., Perovskite thin films via atomic layer deposition. *Advanced Materials* **2015,** *27* (1), 53-58.

66. Chen, Q.; Zhou, H.; Hong, Z.; Luo, S.; Duan, H.-S.; Wang, H.-H.; Liu, Y.; Li, G.; Yang, Y., Planar heterojunction perovskite solar cells via vapor-assisted solution process. *Journal of the American Chemical Society* **2013,** *136* (2), 622-625.

67. Moore, D. T.; Sai, H.; Tan, K. W.; Estroff, L. A.; Wiesner, U., Impact of the organic halide salt on final perovskite composition for photovoltaic applications. *APL Materials* **2014,** *2* (8), 081802.

68. Williams, S. T.; Zuo, F.; Chueh, C.-C.; Liao, C.-Y.; Liang, P.-W.; Jen, A. K.-Y., Role of chloride in the morphological evolution of organo-lead halide perovskite thin films. *ACS nano* **2014,** *8* (10), 10640-10654.

69. Saliba, M.; Tan, K. W.; Sai, H.; Moore, D. T.; Scott, T.; Zhang, W.; Estroff, L. A.; Wiesner, U.;

Snaith, H. J., Influence of thermal processing protocol upon the crystallization and photovoltaic performance of organic–inorganic lead trihalide perovskites. *The Journal of Physical Chemistry C* **2014,** *118* (30), 17171-17177.

70. Liang, P. W.; Liao, C. Y.; Chueh, C. C.; Zuo, F.; Williams, S. T.; Xin, X. K.; Lin, J.; Jen, A. K. Y., Additive enhanced crystallization of solution-processed perovskite for highly efficient planar heterojunction solar cells. *Advanced Materials* **2014,** *26* (22), 3748-3754.

71. Zuo, C.; Ding, L., An 80.11% FF record achieved for perovskite solar cells by using the NH4Cl additive. *Nanoscale* **2014,** *6* (17), 9935-9938.

72. Chen, C.-C.; Bae, S.-H.; Chang, W.-H.; Hong, Z.; Li, G.; Chen, Q.; Zhou, H.; Yang, Y., Perovskite/polymer monolithic hybrid tandem solar cells utilizing a low-temperature, full solution process. *Materials Horizons* **2015,** *2* (2), 203-211.

73. Zhou, H.; Chen, Q.; Li, G.; Luo, S.; Song, T.-b.; Duan, H.-S.; Hong, Z.; You, J.; Liu, Y.; Yang, Y., Interface engineering of highly efficient perovskite solar cells. *Science* **2014,** *345* (6196), 542-546.

74. You, J.; Yang, Y. M.; Hong, Z.; Song, T.-B.; Meng, L.; Liu, Y.; Jiang, C.; Zhou, H.; Chang, W.-H.; Li, G., Moisture assisted perovskite film growth for high performance solar cells. *Applied Physics Letters* **2014,** *105* (18), 183902.

75. Xiao, Z.; Dong, Q.; Bi, C.; Shao, Y.; Yuan, Y.; Huang, J., Solvent Annealing of Perovskite Induced Crystal Growth for Photovoltaic□Device Efficiency Enhancement. *Advanced Materials* **2014,** *26* (37), 6503-6509.

76. Jeon, N. J.; Noh, J. H.; Kim, Y. C.; Yang, W. S.; Ryu, S.; Seok, S. I., Solvent engineering for high-performance inorganic–organic hybrid perovskite solar cells. *Nature materials* **2014,** *13* (9), 897-903.

77. Xiao, M.; Huang, F.; Huang, W.; Dkhissi, Y.; Zhu, Y.; Etheridge, J.; Gray Weale, A.; Bach, U.; Cheng, Y. B.; Spiccia, L., A fast deposition□crystallization procedure for highly efficient lead iodide perovskite thin film solar cells. *Angewandte Chemie* **2014,** *126* (37), 10056-10061.

78. Yang, W. S.; Noh, J. H.; Jeon, N. J.; Kim, Y. C.; Ryu, S.; Seo, J.; Seok, S. I., High-performance photovoltaic perovskite layers fabricated through intramolecular exchange. *Science* **2015,** *348* (6240),

1234-1237.

79. Lee, J. K.; Ma, W. L.; Brabec, C. J.; Yuen, J.; Moon, J. S.; Kim, J. Y.; Lee, K.; Bazan, G. C.; Heeger, A. J., Processing additives for improved efficiency from bulk heterojunction solar cells. *Journal of the American Chemical Society* **2008,** *130* (11), 3619-3623.

80. Peet, J.; Kim, J. Y.; Coates, N. E.; Ma, W. L.; Moses, D.; Heeger, A. J.; Bazan, G. C., Efficiency enhancement in low-bandgap polymer solar cells by processing with alkane dithiols. *Nature materials* **2007,** *6* (7), 497-500.

81. Choi, H.; Park, J. S.; Jeong, E.; Kim, G. H.; Lee, B. R.; Kim, S. O.; Song, M. H.; Woo, H. Y.; Kim, J. Y., Combination of Titanium Oxide and a Conjugated Polyelectrolyte for High Performance Inverted□Type Organic Optoelectronic Devices. *Advanced Materials* **2011,** *23* (24), 2759-2763.

82. Seo, J. H.; Gutacker, A.; Sun, Y.; Wu, H.; Huang, F.; Cao, Y.; Scherf, U.; Heeger, A. J.; Bazan, G. C., Improved high-efficiency organic solar cells via incorporation of a conjugated polyelectrolyte interlayer. *Journal of the American Chemical Society* **2011,** *133* (22), 8416-8419.

83. Park, S. Y.; Kim, B. J.; Kim, K.; Kang, M. S.; Lim, K. H.; Lee, T. I.; Myoung, J. M.; Baik, H. K.; Cho, J. H.; Kim, Y. S., Low Temperature, Solution Processed and Alkali Metal Doped ZnO for High Performance Thin Film Transistors. *Advanced Materials* **2012,** *24* (6), 834-838.

84. Kwon, S.; Lim, K.-G.; Shim, M.; Moon, H. C.; Park, J.; Jeon, G.; Shin, J.; Cho, K.; Lee, T.-W.; Kim, J. K., Air-stable inverted structure of hybrid solar cells using a cesium-doped ZnO electron transport layer prepared by a sol–gel process. *Journal of Materials Chemistry A* **2013,** *1* (38), 11802-11808.

85. Lee, B. R.; Jung, E. D.; Nam, Y. S.; Jung, M.; Park, J. S.; Lee, S.; Choi, H.; Ko, S. J.; Shin, N. R.; Kim, Y. K., Amine Based Polar Solvent Treatment for Highly Efficient Inverted Polymer Solar Cells. *Advanced Materials* **2014,** *26* (3), 494-500.

86. Nho, S.; Baek, G.; Park, S.; Lee, B. R.; Cha, M. J.; Lim, D. C.; Seo, J. H.; Oh, S.-H.; Song, M. H.; Cho, S., Highly efficient inverted bulk-heterojunction solar cells with a gradiently-doped ZnO layer. *Energy & Environmental Science* **2016,** *9* (1), 240-246.

87. Mahmood, K.; Park, S. B., Highly efficient dye-sensitized solar cell with an electrostatic spray

deposited upright-standing boron-doped ZnO (BZO) nanoporous nanosheet-based photoanode. *Journal of Materials Chemistry A* **2013,** *1* (15), 4826-4835.

88. Liu, D.; Kelly, T. L., Perovskite solar cells with a planar heterojunction structure prepared using room-temperature solution processing techniques. *Nature photonics* **2014,** *8* (2), 133-138.

89. Xu, F.; Sun, L., Solution-derived ZnO nanostructures for photoanodes of dye-sensitized solar cells. *Energy & Environmental Science* **2011,** *4* (3), 818-841.

90. Mahmood, K.; Park, S. B.; Sung, H. J., Enhanced photoluminescence, Raman spectra and field-emission behavior of indium-doped ZnO nanostructures. *Journal of Materials Chemistry C* **2013,** *1* (18), 3138-3149.

91. Saliba, M.; Matsui, T.; Seo, J.-Y.; Domanski, K.; Correa-Baena, J.-P.; Nazeeruddin, M. K.; Zakeeruddin, S. M.; Tress, W.; Abate, A.; Hagfeldt, A., Cesium-containing triple cation perovskite solar cells: improved stability, reproducibility and high efficiency. *Energy & Environmental Science* **2016,** *9* (6), 1989-1997.

92. Yang, J.; Siempelkamp, B. D.; Mosconi, E.; De Angelis, F.; Kelly, T. L., Origin of the thermal instability in CH3NH3PbI3 thin films deposited on ZnO. *Chemistry of Materials* **2015,** *27* (12), 4229-4236.

93. Song, J.; Hu, W.; Wang, X.-F.; Chen, G.; Tian, W.; Miyasaka, T., HC (NH 2) 2 PbI 3 as a thermally stable absorber for efficient ZnO-based perovskite solar cells. *Journal of Materials Chemistry A* **2016,** *4* (21), 8435-8443.

94. Jeon, N. J.; Noh, J. H.; Yang, W. S.; Kim, Y. C.; Ryu, S.; Seo, J.; Seok, S. I., Compositional engineering of perovskite materials for high-performance solar cells. *Nature* **2015,** *517* (7535), 476-480.

95. Gonzalez-Pedro, V.; Juarez-Perez, E. J.; Arsyad, W.-S.; Barea, E. M.; Fabregat-Santiago, F.; Mora-Sero, I.; Bisquert, J., General working principles of CH3NH3PbX3 perovskite solar cells. *Nano letters* **2014,** *14* (2), 888-893.

96. Brown, P. R.; Lunt, R. R.; Zhao, N.; Osedach, T. P.; Wanger, D. D.; Chang, L.-Y.; Bawendi, M. G.;

Bulovic, V., Improved current extraction from ZnO/PbS quantum dot heterojunction photovoltaics using a MoO3 interfacial layer. *Nano letters* **2011,** *11* (7), 2955-2961.

Acknowledgement

It is pleasure to thank the many people who have made the completion for my MS research project possible. Among them, I would like to sincerely thank to my advisor, Prof. Jin Young Kim, for his patience and guidance with his trust and belief. He always gave me chances and supported me. I also thank my committee members, Prof Hye Sung Park, Prof. Sang Il Seok who deserve professional advice.

I'm also thankful to my laboratory NGEL members, Dr. Bright Walker, Dr. Gi-Hwan Kim, Taehyo Kim, Hye-Rim Yeom, Jaeki Jeong, Hak-beom Kim, Seyoung Song, Jungwoo Heo, Song Yi Park, Tack Ho Lee, Kang Taek Lee, Young Jin Yoon, Na Gyeong Ahn, Jaewon Kim, Hyung Su Jang, and Yun Seop Shin. Especially, I would like to thank to perovskite team members, Jaeki and Hak-beom who help me from beginning of my research program. For this research project, I would appreciate Kang Taek who provided ZnO NPs, Young Jin who repeatedly measured the UPS, Jaewon who helped to measure the EIS, Hyung Su who provided MAI and Yun Seop Shin who always helped me. I am also grateful my friends, Yuna, SaetByeol, JiEun, and Sojeong who support me.
I hope to express my gratitude to someone who support me when my difficult time. I could finish the MS program with their support.

I'm very thankful and would like to express my love to my family; my father, mother, YeonJu, and DongJu who always trust and support me. I can finish BS and MS Program in UNIST with their endless love and support. I am also grateful my friends

The time at UNIST has been a great part of my life.